Interrelations between surface, boundary layer, and columnar aerosol properties over a continental urban site

Dongxiang Wang[1], Dominika Szczepanik[1], Iwona S. Stachlewska[1]

[1]University of Warsaw, Faculty of Physics, Institute of Geophysics, Warsaw, 02-093, Poland

Correspondence to: Iwona S. Stachlewska (iwona.stachlewska@fuw.edu.pl)

Abstract. PollyXT Raman Polarization Lidar observations were performed at the Remote Sensing Laboratory (RS-Lab) in Warsaw (52.2109°N, 20.9826°E), Poland, in the framework of the European Aerosol Research Lidar Network (EARLINET) and the Aerosols, Clouds and Trace gases Research Infrastructure (ACTRIS). Data collected in July, August and September of 2013, 2015 and 2016 were analysed using the classical Raman approach. In total 246 sets of profiles, each comprising wavelength dependent particle extinction and backscatter coefficients and linear particle depolarization ratios at 355 nm and 532 nm, as well as water vapour, were derived for statistical investigations (EARLINET/ACTRIS Data Base). The main analysis was focused on intensive optical properties obtained within summertime and early autumn aerosol boundary layer (ABL). The interrelations of different optical properties inside ABL are discussed for different periods: entire day, nocturnal time (with respect to NL nocturnal and RL residual layer), at sunrise (MTL morning transition layer), and from late afternoon till sunset (WML well mixed layer). In addition, the lidar derived daytime boundary layer optical properties (for MTL and WML) were compared with the corresponding columnar daytime aerosol properties derived from shadowband radiometer (MFR-7, PolandAOD-NET) and sunphotometer (CE318, AERONET). High linear correlation of columnar aerosol optical depth for the two latter instruments operated in Warsaw was obtained (R=0.98, st.dev. 0.02). Contribution of the long-range transported aerosol in free troposphere over Warsaw can results in twice higher AOD_{CL} than AOD_{ABL}. Occurrence of turbulence driven aerosol burst from boundary layer to free troposphere can result in increasing this difference. Aerosol composition within ABL and in the free troposphere was assessed based on the derived properties interpreted with respect to values reported in literature as characteristic for different aerosol type and the interpreted against backward trajectories and satellite data. It consisted either of pure urban anthropogenic pollution aerosols (~ 61%), its mixtures with biomass burning aerosols (< 14%), local pollen (< 7%) or arctic marine particles (< 5%). No significant contribution of mineral dust in boundary layer was found. Within boundary layer, the lidar derived optical properties (entire day, 246 sets) revealed the mean aerosol optical depth (AOD_{ABL}) of 0.20±0.10 at 355 nm and 0.11±0.06 at 532 nm; the mean Ångstrom exponent ($ÅE_{ABL}$) of 1.54±0.37; the mean lidar ratio (LR_{ABL}) of 48 ±17 sr at 355 nm and 41±15 sr at 532 nm; the mean linear particle depolarization ratio (δ_{ABL}) of 0.02±0.01 at 355 nm and 0.05±0.01 at 532 nm, the mean water vapour mixing ratio (WV_{ABL}) of 8.28±2.46 g/kg. The lidar derived aerosol boundary layer height (ABLH) and the lidar derived AOD_{ABL} exhibit positive correlation (~ 0.74), associated with local anthropogenic pollution (this being most pronounced for RL and WML). The ABLH and the columnar radiometer/photometer AOD_{CL} show weak negative correlations (-0.28 to -0.36), attributed

to likely influence of smoke advection and/or pollution brust events causing suspended aerosol layers in the free troposphere above the site. This negative trend of ABLH and AOD_{CL} manifested for the summer and early-autumn season in Warsaw; for annual data it is not expected. At this time of year, a positive correlation of AOD_{ABL} and LR_{ABL} and a negative correlation $ÅE_{ABL}$ and LR_{ABL}, as well as expected negative trends in WV_{ABL} and RH versus $\delta_{ABL,}$ were observed. Relations of the aerosol properties and surface in-situ measurements of particulate matter with an aerodynamic diameter < 10µm (PM_{10}) and < 2.5µm ($PM_{2.5}$) (WIOS Network) and the fine to coarse mass ratio (FCMR) are investigated. For MTL and WML the relation between FCMR and surface RH showed positive correlation (0.71 and 0.63, respectively), what was seen even for nighttime (0.6), the latter generally lacking statistically significant relations. A weak negative-correlation of FCMR and δ_{ABL} (more pronounced at 532 nm, nighttime) and no casual relation between FCMR and $ÅE_{ABL}$ was found. Most interesting differences were observed for the sunrise morning transition MTL ranging up to 0.6-1 km, characterised by lower AOD_{ABL} <0.12, with more wet condition RH 60-80%, smaller particles with $ÅE_{ABL}$ of 1-2 and FCMR from 0.5 to 3, and low LR_{ABL} of 20-40 sr. For the well mixed layer WML ranging up to 1-2.5 km, with higher AOD_{ABL} reaching up to 0.45, drier conditions RH 30-60%, comprising larger particles ÅE of 0.8-1.7 and FCMR of 0.2-1.5, and higher LR_{ABL} up to 90 sr.

Keywords: lidar; aerosol boundary layer; aerosol optical properties; particulate matter; near-surface relative humidity,

1 Introduction

Atmospheric aerosols play a significant role in local and global climate and weather change. Aerosols affect the earth radiative budget, as they interact with the incoming solar short-wave radiation and the outgoing terrestrial long-wave radiation. Depending on the aerosol type, they can scatter or absorb the radiation, thus causing warming or cooling the atmosphere locally, at the surface and at the top of atmosphere (Kaufman et al., 2002). The variety of aerosol sources, those of natural and anthropogenic origin, as well as the influence of diverse meteorological conditions on their characteristics and transport, lead to aerosol contents strongly variable in the troposphere. Accordingly to the Inter-governmental Panel on Climate Change (Stocker et al., 2013), the sparse and/or poorly-known information on aerosol temporal and spatial variability causes high uncertainty in the assessment of their influence on the global radiation budget. To improve forecasts of global climate change, it is essential to reduce these uncertainties. Aerosol properties are one of the important parameters in aerosol studies, being useful for radiative transfer, environment and health studies. Aerosol optical properties, size and composition are also important for aerosol-cloud-radiation interaction studies.

Air pollution is one of the major environmental issues in metropolitan areas due to its adverse effects on human health (e.g. Chen et al., 2008, Lelieveld et al., 2015). Air quality is related to anthropogenic emissions, natural emissions and climate change (e.g. Juda-Rezler et al. 2012). Strong emissions, e.g., from traffic, industry or heating, can drastically decrease air quality, particularly when the emitted pollutants ~~are captured below an inversion~~ and when meteorological conditions prevent an exchange of polluted and clean air, (Juda-Rezler et al. 2011). In Europe, surface particulate matter with an aerodynamic diameter below 10µm (PM_{10}) is

one of the most serious air quality problems (De Leeuw et al., 2001). As atmospheric aerosols also affect air quality, health and environment, joint studies of aerosol optical properties in combination with PM can improve our knowledge on atmospheric environment.

The boundary layer affects the dispersion of pollutants within the mixing layer (Wałaszek et al., 2018). The knowledge on boundary layer characteristics and its dynamics, both related to ambient meteorological conditions, is helpful to model and predict mechanisms that matter in weather forecasting, air pollution and climate change studies (Barlage et al., 2016). Therefore, it is meaningful to acquire the knowledge of the ABL top height distribution along with the aerosol optical properties within the ABL.

Lidar techniques seem to be an optimal tool to provide height-resolved aerosol data products. Several lidar techniques are suitable for aerosol studies and in the last ten years rapid progress in laser technology, measurement techniques, and data acquisition systems has contributed to a much wider use of these techniques also for aerosol monitoring, ranging from the simple elastic backscatter lidar / ceilometer networks (Flentje et al., 2010) to the most advanced multi-wavelength Raman lidar system networks (Baars et al., 2016). The European Aerosol Research Lidar Network (EARLINET; https://www.earlinet.org) conducts lidar observations and provides relevant sets of lidar data products stored in a comprehensive, quantitative, and statistically significant database for the aerosol distribution over Europe (Pappalardo et al., 2014). Quality assurance program (Freudenthaler et al., 2018) and lidar data evaluation algorithms (Böckmann et al., 2004) have been developed and assessed at each lidar station, as well as during the lidar intercomparison campaigns (e.g. Wandinger et al., 2016) to meet accuracy standards desired in aerosol radiative forcing need. The unique data set of lidar observations conducted over Europe allows for classification of the aerosol type (e.g. Nicolae et al., 2018, Papagiannopoulos et al., 2018) The EARLINET network is an integral part of the Aerosols, Clouds and Trace gases Research Infrastructure (ACTRIS; https://www.actris.eu) - a pan-European initiative consolidating actions amongst European partners producing high-quality observations of aerosols, clouds and trace gases. As different atmospheric processes are increasingly in the focus of many societal and environmental challenges, such as air quality, health, sustainability and climate change, ACTRIS initiatives aim to contribute in the resolving of challenges by providing a platform for researchers to combine their efforts more effectively, and by providing observational data of aerosols, clouds and trace gases openly to other external users.

The aerosol optical properties derived for boundary layer from lidar have been studied in a statistical approach at several EARLINET sites in Europe (e.g. Mattis et al., 2004, Amiridis et al., 2005, Matthias et al., 2004, Sicard et al., 2011, Siomos et al., 2018). However, studies regarding extensive Raman-lidar derived sets of optical properties, such as wavelength dependent aerosol lidar ratios, optical depths, depolarization ratios, completed with Ångstrom exponent and water vapour content, as compared and interpreted against surface particulate matter and columnar optical properties of are still rare and based on a case study approach (Stachlewska et al., 2017a, 2018, Ansmann et al., 2018, Hu et al., 2019). Combination of such study with hygroscopic growth monitoring is the next step in the future (Navas Guzmán et al., 2019).

In the framework of the EARLINET, extensive observations at a continental, urban site in Warsaw at the Remote Sensing Laboratory (RS-Lab) of the Institute of Geophysics at Faculty of Physics at University of Warsaw have been performed since July 2013. Within this paper the data products of this site published in the EARLINET/ACTRIS Data Base will be utilized (Earlinet

Publishing Group, 2018). The paper deals with the aerosol optical properties derived within boundary layer from the complex Raman lidar, obtained in atmospheric column by radiometer and sunphotometer, and with the particulate matter measurements at the surface. Study is designed to investigate relations between boundary layer, columnar aerosol optical properties, water vapour and surface PMs, along with ABL height characteristics. In section 2, the instrumentation and datasets are described. Section 3 presents methodology of boundary layer height derivation and the aerosol optical properties retrieval approaches. Section 4 focuses on comparisons of different types of mean optical properties as derived within boundary layer and in the atmospheric column, PMs, ABLHs and near-surface relative humidity. Conclusions are given in section 5.

2 Instrumentation and data set

The PollyXT Raman polarization and water-vapor lidar (52.2109°N, 20.9826°E, 112 m a.s.l.) is located at the Remote Sensing Laboratory (RS-Lab, https://www.igf.fuw.edu.pl/en/instruments) of the Institute of Geophysics at the Faculty of Physics of the University of Warsaw, Poland. Location of the RS-Lab is denoted in Figure 1. The RS-Lab conducts observations as a part of the European Aerosol Research Lidar Network (EARLINET, www.earlinet.org , Pappalardo et al., 2014), it provides regular measurements within the worldwide Polly.NET lidar network (http://polly.tropos.de/, Baars et al., 2016) and within the National Aerosol Research Network PolandAOD-NET (www.polandaod.pl , supplement material in Markowicz et al., 2016).

Since July 2013, Polly XT lidar performs quasi-continuous 24/7 observations. Powerful laser pulses (180, 110 and 60 mJ) at 1064, 532 and 355 nm are emitted co-axially and vertically, with a 20 Hz repetition frequency, into the atmosphere. Detection is performed with a Newtonian telescope at 8-channels (so-called $2\alpha+3\beta+2\delta+WV$), which enables determination of the particle extinction coefficient profiles (α) at 532 nm and 355 nm, the particle backscatter coefficient profiles (β) at 1064 nm, 532 nm and 355 nm, the particle linear depolarization ratio profiles (δ) at 532 and 355 nm, and water vapour mixing ratio (WV). The signals at all channels are recorded up to 48 km with standard 7.5 m vertical resolution in temporal steps of 30 s. Measured signals are affected by an incomplete geometrical overlap between the emitted laser beam and the full field of view of the lidar telescope, and therefore the signals in the range below 400 m altitude are rejected from further evaluation. The lidar is described in a great detail in Engelmann et al (2016). The incomplete overlap-range issue posed a first constrain on the selected dataset, i.e. constraining analyses to summer and early-autumn data. In winter, the atmospheric boundary layer height derived at noon and midnight from the radiosounding profiles can be found below the complete lidar's overlap range (i.e. the range in which the lidar laser beam is fully received by the field of view of the lidar telescope), and thus the detection of the boundary layer height by lidar is limited in winter. In contrast, in summer and early-autumn, the boundary layer height is always above the complete lidar's overlap range, and thus not affecting the profiles. Therefore, we restricted the analyses of the optical properties within boundary layer the latter seasons.

Quality checked profiles of optical properties are stored in the EARLINET/ACTRIS Data Base (www.earlinet.org). The statistical analysis covers profiles derived for EARLINET regular measurements (Mondays and Thursdays with ± 2 hours from zenith and sunset) and for dedicated measurements (e.g. diurnal cycles, special alert events). From Warsaw site, only cloud-screened profiles

evaluated using the classical Raman-approach are feed into the Data Base. The profiles obtained for lidar observations in July, August and September in the year of 2013, 2015 and 2016 were analysed (2014 was excluded from analyses due to too sparse data availability). In total, 246 lidar profiles were collected for this study (denoted as contributing to *entire time*), whereby 113 profiles were obtained for *nocturnal time* (21:00-02:00 UTC) and 37 profiles were derived at sunrise (03:00-08:00 UTC) and 63 profiles at sunset (16:00-20:00 UTC), here defined as the *sunrise/sunset or transition time*. The precise sunrise and sunset times are available via www.timeanddate.com/sun/poland/warsaw. Note, that only 29 profiles were available at daytime conditions (08:00-16:00 UTC), which was considered as too low number to consider separately category of day time, i.e. these profiles join category entire time. The analysed time is separated into three periods because the change of atmospheric conditions is driven by different processes during those times, allowing therefore a possibility to search for and signature of aerosol optical properties change. However, comparisons of the optical properties derived from lidar and photometer were done for a subset of daytime profiles (03:00-19:00 UTC).

Multi-Filter Rotating Shadowband Radiometer (MFR-7; Yankee Environmental Systems) was used for continuous passive measurements at the RS-Lab in the frame of the PolandAOD-NET network activities. The instrument operates at six narrow-band channels (415, 500, 610, 675, 870 and 940 nm) and one broadband channel. It measures direct, diffuse and total solar radiation from which the spectrally resolved aerosol optical depth is obtained. In-situ calibration using the classic Langley approach is applied on regular basis. Details on the instrument design and uncertainty analyses are reported in Harrison et al. (1994). Cloud-screened products used in this study are: $AOD_{CL}(415)$ and $AOD_{CL}(500)$ with uncertainty at the level of ±0.025., and $ÅE_{CL}(415/500)$ with uncertainty at the level of ±0.04. There is a threshold on the values of AOD_{CL} <0.03, being excluded from analyses.

Sun-photometer (CE318; CIMEL Electronique) operates at Polish Academy of Science Observatory in Belsk (51.8366°N, 20.7916°E, 190 m a.s.l.), located 43.7 km south-west of the RS-Lab in Warsaw providing longest record of passive measurements in Poland. The same instrument was recently installed in RS-Lab in Warsaw and since January 2018 provides data to AERONET. Passive measurements of direct and diffuse solar irradiance and sky radiance at the Earth's surface at nine wavelengths in a spectral range from 340 nm to 1640 nm are used for retrieval of AOD and ÅE. The data are calibrated once a year at PHOTONS/AERONET-EUROPE calibration centre (http://loaphotons.univ-lille1.fr) and processed by the Aerosol Robotic Network (AERONET, http://aeronet.gsfc.nasa.gov, Holben et al., 1998). Products used in this study: AERONET Level 2.0 cloud-screened $AOD_{CL}(380)$ and $AOD_{CL}(500)$ with uncertainty at the level of ±0.01., and $ÅE_{CL}(380/500)$ with uncertainty at the level of ±0.03. There is a threshold on the values of AOD_{CL} <0.03, being excluded from analyses. Note that, the AOD_{CL} from MFR-7 and CE813 are scaled using the Ångstrom law (Ångstrom, 1929, Iqbal, 1983) to match the lidar wavelength. As for the CIMEL, it is located about 2 km from the village of Belsk in a typical agricultural region with fertile soil and trees. Note that the AERONET data in Belsk were used in the current study only for data consistency check and only as an indicative that the free tropospheric aerosol load existed above Warsaw and in its vicinity. Therefore, Belsk data do not contribute to the core results.

Particulate matter concentrations for particles with an aerodynamic diameter of less than 2.5μm and 10μm (denoted $PM_{2.5}$ and PM_{10}, respectively) were measured at the air-quality monitoring site of the Warsaw Regional Inspectorate of Environmental

Protection (WIOS) in Warsaw-Ursynow, located 6.5 km from the RS-Lab. The PM site is in the residential area of Ursynow (about 6.5 km south from RS-Lab). The RS-Lab is located at the University campus shrouded by green parks. Between the three sites there is no possible industrial pollution sources; anthropogenic pollution in summertime is related to traffic.

The daily and hourly averaged $PM_{2.5}$ and PM_{10} data are visualised via http://sojp.wios.warszawa.pl/raport-dobowy-i-roczny. The data measurements conducted at the stations of State Environmental Monitoring are gathered in the Air-Quality database JPOAT 2,0 of the National Chief Inspectorate for Environmental Protection (GIOS). This official, calibrated datasets of $PM_{2.5}$ & PM_{10} are accessible via http://powietrze.gios.gov.pl/pjp/archive. The measurement uncertainty is below 30% for the hourly concentrations. Products used in this study: surface daily and hourly mean particulate matter concentrations for $PM_{2.5}$ and PM_{10}, and the fine-to-coarse mass ratio (FCMR) defined as $PM_{2.5}/(PM_{10}-PM_{2.5})$ (Zawadzka et al., 2013). FCMR > 1.5 denotes *fine particles* domination (diameter < 2.5μm); FCMR < 0.5 means *coarse particles* domination (diameter between 2.5 μm to 10 μm). Values in the range of 0.5 < FCMR< 1.5 indicate that fine and coarse particles are distributed approximately equally.

The temperature, pressure, relative humidity, wind speed and direction at the surface (p, T, RH, V, Vdir), were measured by the weather transmitter WXT510 (Vaisala) mounted on the roof platform of the RS-Lab at 21 m above the ground's surface. The atmospheric pressure, temperature and relative humidity profiles are obtained from the radiosonde RS92 (Vaisala) launched at two World Meteorological Organization sites located in Poland: WMO 12374 station in Legionowo (52.40°N, 20.96°E, 96 m a.s.l., 25 km North of Warsaw) and WMO 12425 station in Wroclaw (51.78°N, 16.88°E, 122 m a.s.l., 300 km South-West of Warsaw). The noon and midnight radiosounding profiles (launch at 11:15 / 23:15 UTC, duration of circa 1.5 h) were visualized and downloaded via the University of Wyoming Upper Air Data website (weather.uwyo.edu/upperair/sounding.html).

Note that the shadowband and the sunphotometer derived AOD and the in-situ measured PM values are averaged with corresponding time of the lidar-derived optical profiles available for given period for the Warsaw site in the EARLINET/ACTRIS Data Base. Moreover, MFR-7 and CE318 collected data only at daytime. The measurement sites are showed in Figure 1.

3 Methodology of lidar products retrieval

The atmospheric boundary layer is regarded as the lowest layer of the troposphere, being directly influenced by the Earth's surface and reacting quickly to the surface forcing. The atmospheric boundary layer under well-mixed conditions in summer and early-autumn can be characterized as a layer efficiently trapping aerosol particles in it (as in comparison with winter boundary layer). The lidar mean derived aerosol boundary layer height in Warsaw for July, August and September of 2013, 2015 and 2016, is of 1.48±0.65km, 1.34±0.56km, 0.98±0.54km, which is significantly higher than winter mean value of 0.64±0.43 km. Therefore, the chosen time period is expected to be in significant relation with the lidar derived aerosol boundary layer height (ABLH). The latter is derived from the lidar elastic-scattering aerosol backscatter signal, relying on a higher aerosol load within the boundary layer than in the free troposphere. Wang et al. (2018) demonstrated that for the PollyXT lidar data in Warsaw ABLHs derived using the wavelet covariance transform method (WCT) give optimal results. The WCT calculations are applied for ABLH estimations as in Wang et al. 2018, with slight modification of the methodology: i) the dilation of 30 range-bins is applied on

signals averaged over 7.5 m and 30 min; and ii) the ABLH is derived at all three elastic wavelengths (355, 532 and 1064 nm), and then averaged for a final result.

Lidar signals stored in the EARLINET/ACTRIS Data Base were evaluated using the classical Raman retrieval approach. The particle extinction coefficient profiles at 355 and 532 nm are calculated from the so-called Raman lidar equation using the Rayleigh law for molecules and the Ångstrom law (usually with ÅE=1) for aerosol particles. The particle backscatter coefficient profiles at 355, 532 and 1064 nm are derived with the use of the obtained particle extinction coefficient profiles at 355 nm and 532 nm (used for both larger wavelengths) and calibrated at the height range free of aerosol. More details on the exact procedure is given in Baars et al. (2016). The procedure for the ±45 depolarization calibration method is used as in Engelmann et al. 2016. The water vapour was obtained by the ratio of Raman water vapor channel and Raman nitrogen channel, described in Stachlewska et al. (2017a).

For all analysed data products, low- and mid-altitude clouds are screened prior to the retrieval. The profiles of the particle extinction and backscattering coefficients, and particle linear depolarization ratio were averaged over 60min (60%) or 45min (23%) or 30min (17% of profiles), depending on the atmospheric conditions variability and the signal-to-noise ratio, and smoothed with running mean over 49 range-bins (length of single range-bin is 7.5 m). The profiles of the water vapour mixing ratio were averaged over 30-60 min and 60 m with no smoothing applied. In lidar retrieval, the atmospheric profiles of pressure, temperature, relative humidity obtained by RS92 at Legionowo (WMO12374, site) or Wroclaw (WMO 12425 site), depending on the approaching direction of the air-mass transport were used.

After having determined ABLH, the mean values of different optical properties within the boundary layer are derived. However, for the incomplete overlap region, special care of the data in lowermost altitude range have to be applied. The lowest value of available particle extinction coefficient was assumed as representative down to the ground surface; this being commonly accepted approach in lidar studies, e.g. Matthias et al. (2004). Therefore, the mean extinction coefficient of the entire ABL is obtained by extrapolating the extinction profile with this value down to the ground. Similarly, the mean backscattering coefficient and the particle depolarization ratio of ABL. The δ profiles can be derived almost to the ground, however for the EARLINET/ACTRIS Data Base profiles are stored down to 400 m, so that extrapolation also here is required. The water vapour mixing ratio profiles were also extrapolated from 100 m down to the ground. The water vapor mixing ratio profile is calculated using the ratio of two signals at 407 and 387 nm Raman channels. The overlap term of those two channels (close in spectral range; only 20 nm) practically cancels when calculating their ratio. Similarly, for the particle depolarization ratio (of cross channel and corresponding total channel at the same wavelength), the overlap term also cancels. Therefore, the water vapor (so as the depolarization ratio profile can be obtained almost down to the ground. Water vapour nighttime detection in June-September is typically performed from 20:00 to 4:00 UTC, thus only the data corresponding to nocturnal time (21:00 to 2:00 UTC) were analysed.

Additionally, within ABL, the vertical distribution of the lidar ratio (LR_{ABL}) was derived as a ratio of the aerosol extinction to backscatter coefficient profiles at 355 and 532 nm, and then the mean LR_{ABL} are calculated. The vertical distribution of the Ångström exponent $ÅE_{ABL}$(355/532) was computed by the means of using the profiles of aerosol extinction coefficient (not AOD) at 355 and 532 nm, then mean $ÅE_{ABL}$ is calculated. The aerosol optical depth (AOD_{ABL}) has been calculated by integrating the

extrapolated aerosol extinction profile derived with the lidar at 355 and 532 nm. There is a threshold set on the mean values of $AOD_{ABL}(355) < 0.05$ and $AOD_{ABL}(532) < 0.03$ within lowermost 1 km, i.e. aerosol extinction coefficient profiles are extrapolated according to the AOD threshold for each wavelength. If AOD within 1 km is below the threshold, re-extrapolation is applied from a range-bin just above the initially chosen one down to the ground in an iterative manner until the AOD values within 1 km meet the given above thresholds. Stachlewska et al. (2018) reported the uncertainty of AOD_{ABL} at 355 and 532 nm derived from the Raman extinction coefficient profiles < 20%, the uncertainty of LR_{ABL} derived by extinction-to-backscattering coefficient ratios at 355 and 532 nm < 35%, and the uncertainty of δ_{ABL} at 355 and 532 nm < 20% of derived value. The uncertainty of extinction-derived $ÅE_{ABL}(355/532)$ is < 30% The uncertainty of the ABLH retrieval from PollyXT lidar are of ±40 m (Wang et al., 2018).

The aerosol within boundary layer and in the layers in free troposphere is interpreted using the values of the optical properties (LR, δ, ÅE, RH) as reported in literature (an excellent review of those is provided by e.g. by Nicolae et al., 2018), wherby the range of used values is indicated in Table 1.

Roughly speaking, LR > 75 sr indicate existence of particles related to biomass burning, 40-50 sr mineral dust, 50-60 sr anthropogenic pollution, and 20-30 sr arctic marine particles.

Particle linear depolarization ratio (δ) is used as an indicator of atmospheric anisotropy and tracer of non-spherical particles, roughly speaking, low values of δ < 0.01 are regarded as due to very small spherical particles in the atmosphere (e.g. pure pollution). Values of δ in the range of 0.2-0.35 are characteristic for pure dust; polluted dust values are lower, down to even 0.1. Values in range of 0.04-0.08 are regarded as for biomass burning aerosol), then for pollen ~ 0.1, and for urban pollution < 0.2.

The Ångstrom exponent (ÅE) was used as an indicator of the size of atmospheric aerosols. Values of ÅE ≤ 1 indicate particle size distributions dominated by the coarse-mode aerosols (radii ≥ 0.5 μm, here called *large particles*) that are typically associated with dust and sea salt particles (Perrone et al. 2014). Values of ÅE ≥ 1.5 indicate size distributions dominated by the fine-mode aerosols (radii < 0.5 μm, here called *small particles*) that are associated with urban pollution (Perrone et al. 2014). Values within the range of 1< ÅE < 1.5 belong to accumulation-mode (here called *medium-size particles*) and are associated with biomass burning aerosol (Janicka et al., 2017, 2019). Use of the ÅE nomenclature of *small, medium, and large* size particle is for clarity, as not to confuse them with the fine-to-coarse mass ratio (FCMR).

4 Results and discussion

Table 2 shows the mean extinction coefficient (α), backscatter coefficient (β), aerosol optical depth (AOD), lidar ratio (LR), particle linear depolarization ratio (δ) and Ångstrom exponent (ÅE) derived at 355 and 532 nm channels within the aerosol boundary layer (ABL) for the entire (ET), nocturnal (NT) and Transition (TT) time derived for measurement period July-September, 2013, 2015, and 2016. Different mechanisms govern the sunrise and sunset conditions; the first is driven by development of convective boundary layer and the latter lessens convection to prone stratification with residual layer (RL). As the developed ABLH algorithm determines the aerosol boundary layer top as a well-mixed layer (WML), a nocturnal layer (RL)

and/or a residual layer (RL), for the sunrise/sunset time it is used for data interpretation. The mean ET ABLH was of 1.33±0.36 km for this period. For comparison, Wang et al. (2018) demonstrated, based on the 10-years data set, that the decadal mean ABLH in Warsaw exhibits a clearly higher value in summer than in other seasons, whereby the mean summer ABLH was of 1.24±0.64 km in 2013, 1.80±0.60 km in 2015 and 1.57±0.67 km in 2016.

The mean values of α_{ABL}, AOD_{ABL} and LR_{ABL} calculated at the two wavelengths are very similar in entire and nocturnal time, while corresponding values in transition time are higher than sunset for WML and lower for MTL, the latter being similar to NL for the two other periods. This indicates that the convective mixing and the change of atmospheric conditions impact light extinction on aerosol particles within the ABL. In general, the mean $ÅE_{ABL}$ was high (1.37-1.61), indicating small-size particles. In nocturnal period, $ÅE_{ABL}$ values are higher than for the other periods, indicating that even smaller particles occur at the nighttime during summer and early-autumn in Warsaw. ~~However this does not necessarily mean that pollution is intensifying at night, as it may be related to less intense traffic, lack of photo-smog, and cooling at the ground surface at night.~~

The frequency distribution plots for the AOD_{ABL}, LR_{ABL}, $ÅE_{ABL}$ derived at 355 and 532 nm and the FCMR derived for $PM_{2.5}$ and PM_{10} for the entire, nocturnal and sunrise/sunset times are shown in Figure 2. The mean AOD_{ABL} mainly ranges from 0.1-0.3 at both wavelengths during three periods. Above 80% of occurrence is attributed to $AOD_{ABL}(355)$ in the range of 0.1-0.3 and $AOD_{ABL}(532)$ of below 0.3. The values of mean $LR_{ABL}(355)$ and $LR_{ABL}(532)$ mainly distribute from 30 to 70 sr, which accounts for more than 75% of total data, whereby frequency distributions of both are very similar for ET and NT-RL. The majority of the $ÅE_{ABL}(355/532)$ values are 1.0-2.0 (more than 90% of total data), which indicates mid- and small-size particles (≤ 500 nm) within boundary layer. On the other hand, the FCMR values between 0.5 and 1.5 constitute around 70% of total data, indicating a more-less equal distribution to fine and coarse particles with a size between 2.5 and 10 µm at the surface. The most of AOD_{ABL} of MTL is below 0.2 at two wavelengths, the mainly LR_{ABL} of MTL is in the range from 25 to 50 sr at 355 and 532 nm. The values of δ_{ABL}in MTL between 0.04-0.06 accounts for around 50 %. The smaller particle in MTL due to the majority of FCMR above 1.5.

Amiridis et al. 2005, reported the 4-years mean AOD_{ABL} of 0.44±0.16 at 355 nm, and the mean LR_{ABL} of 49±25 at 355 nm in summer at Thessaloniki, Greece. According to Papayannis et al. (2008), this much higher value of $AOD_{ABL}(355)$ can be attributed to a significantly stronger impact of the summertime Saharan dust events on Thessaloniki than on Warsaw. Sicard et al. (2011), reported low AOD_{ABL} of 0.07±0.02 at 532 nm in Northeastern Spain, and explained it by the influence of sea-breeze on Barcelona area. Mattis et al. (2004). reported for Leipzig the 3-years mean $AOD_{ABL}(355)$ of 0.38 and $AOD_{ABL}(532)$ of 0.18, with the mean $LR_{ABL}(355)$ of 58 sr and $LR_{ABL}(532)$ of 53 sr, and the mean $ÅE_{ABL}(355/532)$ of 1.4. However, the $ÅE_{ABL}$ was of 1.8-2.2 in the upper boundary layer during summer in Leipzig (Matthias et al., 2004), which is higher than values derived in Warsaw, i.e. during summer slightly larger particles are observed in ABL in Warsaw as compared to Leipzig. Matthias et al. (2004), derived for Raman lidar observations at 10 EARLINET stations: the lowest AOD_{ABL} values in the northwestern (Aberystwyth) and the highest values in the southeastern Europe (Athens), which was again attributed to the impact of Saharan dust events on the aerosol distribution in Southern Europe.

Lidar ratio can be used for the aerosol type characterization. Alados-Arboledas et al. (2011), reported lidar ratios of fresh biomass-burning pollution plume were of 60–65 sr at 355 nm and 532 nm at Granada. Müller et al., (2007), reported the lidar ratios of 45-

60 sr with a mean value of 53 sr at 532 nm, and the particle depolarization ratio <0.05 for Leipzig under local and regional urban and anthropogenic haze conditions. Amiridis et al. (2005) reported for Thessaloniki, the continental aerosol for 4-year mean lidar ratio of 40-47 sr at 355 nm and Giannakaki et al. (2010), the biomass burning aerosols for 7-year mean lidar ratio of 70 sr at 355 nm. Optical properties of eight aerosol types were derived by Burton et al. (2012), derived over North America for the urban aerosol (lidar ratio at 532 nm of 53-70 sr with particle depolarization ratio of 0.03-0.07), and for the smoke particles (lidar ratio of 33-46 sr with particle depolarization ratio of 0.04-0.09). The LR of marine particles with value of 20-26 sr at 532 nm was found in North Atlantic and Tropical Indian Ocean by Müller et al. (2007), and 25±4 sr at 532 nm in Hawaii by Masonis et al. (2003). Dawson et al. (2015) presented the global mean lidar ratio for marine aerosols to be 26 sr, with a range from 22±7 to 32±17 sr, depending on variation of mean ocean surface wind speed. Haarig et al. 2017 reported for the marine particles the lidar ratios varying from 19-27 at 355 nm and 23-25 at 532 nm, and particle depolarization ratio of 0.05-0.12 at 355 and 0.07-0.15 at 532 nm. A review of aerosol types reported by Groß et al., 2013, 2015, include in the classification scheme values based on which: LR for the marine particles varying from 16-30 sr at 355 nm and 18-26 sr at 532 nm, the biomass burning varying from 50-95 sr at 355 nm and 60-90 sr at 532 nm, the mineral dust varying from 50-70 sr at 355 nm and 45-65 sr at 532 nm, the pollution varying from 50-65 sr at 355 nm and 50-60 sr at 532 nm. In current study, for several cases LR_{ABL} in the range of 25-30 sr at both wavelengths was obtained (Figure.2). This is interpreted as likely due to transport of the clean air mass Arctic marine particles into the boundary layer in Warsaw during the analysed period. Such cold air masses can be transported from Arctic to Eastern Europe (Costa-Surós et al. 2015).

Linear particle depolarization ratio is an indicator of non-spherical particles (Ansmann et al. 2009, Sakai et al. 2010, Gasteiger & Freudenthaler. 2014). Generally, the total depolarization ratio in dust episodes are reported above 0.2, while anthropogenic pollution aerosols have a total depolarization ratio below 0.1 (Xie et al., 2008, Nemuc et al., 2013). Heese et al. (2008) reported particle depolarization ratio for dust (~ 0.25) and biomass burning aerosol (< 0.1) over Sahel (West Africa). The particle depolarization ratios of dust particles in the range of 0.1-0.25 were reported in Leipzig (Matthias et al., 2004) and 0.3-0.35 at Ouarzazate, Morocco (Freudenthaler et al. 2009). The particle depolarization ratios of urban haze and fire smoke are reported of less than 0.05 at different sites (Müller et al., 2007). The particle linear depolarization ratio for marine aerosol in the range from 0.01 to 0.03 was reported by Groβ et al. (2011). In the current study, the results of the obtained δ_{ABL} (shown in Figure.2) are within the range of the listed above values characterizing different aerosol types. As δ is sensitive to the size of the sensed non-spherical particles, in particular small-size particles (< 300 nm) sensed with twice larger wavelength (532 nm) can be under detection limit, as seen in Figure.2. The dust cases detected in the free troposphere during the given measurement period in Warsaw (e.g. Janicka et al., 2017) were excluded from analyses (4 cases), yet the derived δ values of entire observation time are less than 0.1, which means that there were no cases of pure dust particles deposited nor advected into the ABL, although polluted dust existence cannot be entirely excluded.

Overall, during period of July to September of 2013, 2015 and 2016 in Warsaw, the aerosol composition within the ABL consisted mainly of urban and anthropogenic aerosols. It was assessed based on derived properties ($ÅE_{ABL}$, WV_{ABL} and

wavelength dependent LR_{ABL} and δ_{ABL}), as interpreted with respect to values reported in literature and with the backward trajectories calculations (plots available via PolandAOD-NET website: www.polandaod.pl).

Firstly, aerosol interpretation was done based on the lidar ratio and secondly, the particle depolarization ratio and the Ångstorm exponent values (Figure 2) against the literature review (summarised in Table 1). Thirdly, the HYSPLIT backward trajectories were calculated to assess the source of aerosol particles of each profile; these were obtained as 3-10 days backward starting at altitude of 0.5, 1.2, and 3 km, applied on GDAS. The estimated aerosol composition consisted mainly of i) pure urban anthropogenic pollution of local origin or transported from areas below or above of the Czech Republic via Silesia and/or Germany (61%), with its mixtures with ii) grass and peatland biomass burning aerosols transported from Russia over Ukraine and Belarus (14%), iii) pollen emissions of strictly local origin form the many semi-natural Warsaw's green parks (7%), iv) arctic marine particles transported mainly from Arctic over Baltic Sea (5%). For remaining cases, identification of aerosol composition was regarded as due to a mixture of more than two sub-components (13%). The given percentage were derived as related to the number of profiles with estimated origin to the total number of profiles, and therefore are given without uncertainties. For remaining cases identification of aerosol composition was regarded as due to a mixture of more that tow sub-component. No significant contribution of mineral dust in boundary layer was found, although transport pathways from Sahara over Iberian Peninsula or via Italy were identified for upper troposphere.

For the collocated Raman lidar measurements with sunphotometer or shadowband radiometer it is interesting to compare the AOD values derived within the boundary layer and in the column of air. Even though such measurements never sample the same air; lidar in zenith-position versus photometer at angles related to Sun's elevation over the horizon. So as to make sure that the columnar measurements with less used in lidar community shadowband radiometer do provide high quality data products intercomparisons of the MFR7 (PolandAOD-NET Level 1.5) and C318 (AERONET Level 2.0) were performed. The use of the specified above level of data for both networks is defined as a clear-sky, manually cloud screened, calibrated within 12 months data product. One month of collocated daytime (03-19 UTC) measurements in July 2018 at RS-Lab in Warsaw was chosen for intercomparisons, which confirmed the high quality of measurements performed using both instruments. The correlation coefficient of daytime AOD at 500 nm was 0.98 with standard deviation of only 0.02 for 114 data points). The results are shown in Figure 3.

Figure 4 shows the daytime mean 30-60 min average of the aerosol optical depth within aerosol boundary layer AOD_{ABL} at 355 and 532 nm, calculated from the mean extinction coefficient profiles of EARLINET PollyXT lidar in Warsaw. For comparison, the columnar daytime mean 1h average (with threshold of at least 5 data points) of the AOD_{CL} at 380 and 500 nm determined from the AERONET CE318 sunphotometer observations in Belsk, AOD_{CL} at 415 and 500 nm derived from the PolandAOD-NET MFR-7 radiometer measurements in Warsaw. Note that, AOD_{CL} of CE318 and MFR-7 were in good agreement with Warsaw results (Belsk values being generally slightly lower than Warsaw, compare Table 3). After that, AOD_{CL} at CE318 and MFR-7 were scaled to 355 and 532 nm using Ångstrom law are plotted. Along with these three, Figure 4 depicts also the $ÅE_{CL}(355/532)$ computed from the AOD_{CL} and extinction-derived $ÅE_{ABL}(355/532)$ of lidar. Products presented in Figure 4 were derived for

period of July to September of 2013, 2015 and 2016, for these cases when all three instruments were conducting observations at the same time (i.e. 41 cases).

In Table 3, the CE318 derived mean AOD is of 0.41±0.17 at 355 nm and 0.23±0.09 at 532 nm, the MFR-7 derived mean AOD is of 0.45±0.17 at 355 and 0.25±0.11 at 532 nm, and the PollyXT derived mean AOD_{ABL} is of 0.20±0.06 at 355 and 0.13±0.03 at 532 nm, for the 41 comparison points. The columnar AOD_{CL} values of the two instruments are the same in the given uncertainty range, despite of the 43.7 km between the two sites. It can be expected that $AOD_{ABL} < AOD_{CL}$ (e.g. Sicard et al., 2011). For a rural site roughly 80% of AOD_{CL} can be assumed as a proxy representative for AOD_{ABL}, e.g. Szczepanik & Markowicz (2018), which is however, not necessarily a valid assumption for the urban sites, e.g. Stachlewska et al. (2017b), especially for conditions with high aerosol load in free troposphere, e.g. Janicka et al. 2017. The obtained results of the mean values of the AOD_{ABL} being 2 times lower than the mean values of AOD_{CL}, indicate that the aerosol layers in the free troposphere in summer and early-autumn over Warsaw, are likely occurring frequently and they significantly contribute to the sensed AOD_{CL}, which is very much in agreement with e.g. Markowicz et al. (2016). This is why, for comparisons in Table.3 in brackets, also the mean values derived for cases of no long-range transport in the free-troposphere are listed, as given in EARLINET/ACTRIS Data Base (i.e. allocation to forest-fire, dust, etc.). Excluding the cases from mean results in lower in AOD_{CL} of roughly 20 to 30 % in Warsaw and 10 % in Belsk; this indicating that must be another source of aerosol over Warsaw. At the same time, for the mean values of summer/early-autumn AOD_{ABL} of 0.20 at 355 nm and 0.13 at 532 nm do not decrease much. Moreover, these are actually rather high values. For conditions with no aerosol layers in the free-troposphere about the site, Szczepanik & Markowicz, (2018) proposed an approximation of boundary layer aerosol load for rural mountainous site (Strzyzow, Poland) as being of AOD_{ABL} (Strzyzow) ≈ 80% AOD_{CL}. Clearly this approximation for Warsaw urban continental site would be not possible.

In a closer look in Figure 4, the lidar derived AOD_{ABL} are of less than 0.2 on a few days, (e.g. case number 9-13), although corresponding values of passive derived AOD_{CL} are more than 0.7. This is not a mistake. On 10 July 2013, the biomass burning aerosol from Canadian wildfires was detected by lidar in Warsaw, with an apparent optically thick aerosol layer suspended in the lower troposphere just above the boundary layer top height, as reported by Janicka et al. (2017) and Ortiz-Amezcua et al. (2017). Due to the low ABLH (< 1000 m) on this day, (not unusual under high pressure system over Poland e.g. Janicka & Stachlewska, Stachlewska et al., (2018), the optical depth contribution of aerosol smoke layer in the free troposphere dominated over the optical depth contribution of the aerosol within boundary layer, which explains much higher columnar than boundary layer AOD. Markowicz et al. (2016), reported existence of aerosol layers in free troposphere with significant (up to 55%) contribution to the total optical depth, which is consistent with results obtained in the current paper.

In general, the results in Figure.4 obtained for the ÅE\as being related to particle size, show that retrievals by all three instruments have similar trend of variation with time. The mean $ÅE_{CL}$ values given in Table 3, are the same, in the given variability range for all 41 cases, despite differences in calculation wavelengths. The values in brackets (no long-range transport of aerosols in free-troposphere, show consistency even higher $ÅE_{ABL}$ than $ÅE_{CL}$ mean values – indication of pollution constrained in boundary layer.

4.1 Relation of ABLH with optical properties and surface PM

The scatter plots of the mean AOD_{CL} and AOD_{ABL} against ABLH for the 41 comparison cases of collocated in time measurements conducted with the MFR-7 and PollyXT, are depicted in Figure 5. The AOD_{CL} and ABLH shows negative trend, while the AOD_{ABL} and ABLH exhibits positive correlation (0.74 at both wavelength); the latter, which is being even higher than the correlation coefficient of 0.55 between AOD_{ABL} and ABLH reported for Leipzig by Mattis et al. (2004) and for Warsaw by Stachlewska et al. (2017b). On the other hand, during stationary high pressure system conditions over Poland, when there is no aerosol in free troposphere above Warsaw but it is injected into boundary layer, both AOD_{CL} and AOD_{ABL} can increase with increasing boundary layer height as e.g. on 24-29 August 2016 (Stachlewska et al., 2017b), even more clearly observed during 10-16 September 2016 (Stachlewska et al., 2018).

The opposite trend in AOD_{CL} – ABLH and AOD_{ABL} – ABLH, is expected to attribute to different type of aerosol load in free-troposphere and/or boundary layer. When aerosol layer containing particles of dust, smoke, pollution or their mixtures is suspended in the free troposphere, an increase of columnar AOD_{CL} values can be observed. Marinou et al. 2017 reported that dust particles can be transported far away from their source of origin and are frequently observed over central and northern Europe, with higher occurrences during summer. High occurrence of the dust particles over Warsaw in spring and summer was also reported by Chilinski et al. 2016 and Janicka et al. 2017. Biomass burning particles and smoke layers were detected over central Europe in summer of 2013 (Janicka et al., 2017, Ortiz-Amezcua et al., 2017, Trickl et al., 2015), of 2015 (Stachlewska et al., 2017b, Szkop & Pietruczuk, 2017), and 2016 (Stachlewska et al., 2018). The dust component and biomass burning were detected and analysed in south Europe with a long record of 10 years lidar dataset (Siomos et al. 2017, 2018). The Canadian wildfire smoke detected in the troposphere and the stratosphere in summer 2017 over central Europe were reported by Haaring et al. (2018) and Ansmann et al. (2018).

The less sufficient growth of the ABLH, can be explained as partly due to the fact that the aerosol layers suspended free troposphere will reduce the solar radiation reaching the surface and suppress the thermal turbulence, leading to lower boundary layer height. Dust layers that can lead to a decreasing of ABLH were reported by several previous studies. The boundary layer decreasing down to 400 m during the Saharan dust intrusion episode in summer at Izaña (South of Spain) was reported by Alastuey et al. (2005). During an intense Saharan dust outbreak in summer, the mixed layer range in the range of 300-400 m in urban area of Barcelona was reported by Pérez et al. (2004). The low mean mixed layer was detected during dust outbreak period at 609±128 m in October in Barcelona by Pandolfi et al. (2013). Hence, for certain conditions the relation of AOD_{CL} and ABLH can be expected to exhibit negative correlation.

By definition, the scatter plot shows spread of the data for which there is no explicate temporal relation, thus the negative correlation does not imply that the decrease in AOD (column) means increase of ABLH, and vice versa. In the 41 cases of daytime measurements (majority of which were taken under clear sky summertime conditions) are related to existence of biomass-burning in free troposphere. In such cases, for lower AOD_{CL} higher ABLH was detected. At the same time, higher AOD_{ABL} is detected for higher ABLH. The two relations are not connected strait forward. Over an urban site that this can be explained as the

AOD_{ABL} grow due to an increase of pollution in urban boundary layer, which adds to the ABLH grow due to Sun-driven turbulence, at the same time the AOD_{CL} decrease would be observed when free tropospheric aerosol load decreases or the type of aerosol present in free troposphere (e.g absorbing aerosols) can cause negative radiative effects at the surface. One more aspect have to be accounted additionally for; the presence of aerosol particles in the troposphere directly above the planetary boundary layer may follow from the dynamics of turbulent eddy structures in the layer. Even in the absence of convection, a typical feature of turbulent boundary layer flows is the presence of abrupt bursting and sweeping events (Pope., 2000). Bursts could eject the aerosol particles from the vicinity of the boundary to upper regions of the boundary layer. The interactions between vortical structures are responsible for the balances of particle concentration in the boundary layer flows (Béghein et al., 2014).

The AOD_{ABL} is an integral of the extinction coefficient within ABLH and the ABLH is a variable of AOD_{ABL}, therefore ABLH is not expected to be strongly related with the aerosol conditions above in the free troposphere. Aerosol optical depth is unique parameter to determine the atmospheric aerosol load and the ABLH derived by lidar is relying on a higher aerosol concentration within the boundary layer than in the free troposphere. Therefore, a positive-correlation of AOD_{ABL} with ABLH, just as observed in Figure 5 can be expected. Note, that although an intrusion of biomass burning smoke into the ABL can contribute strongly to suppression of the growth of ABLH, as reported by Stachlewska et al. (2018), it still does not result in negative correlation.

The relations of lidar derived AOD_{ABL}, $ÅE_{ABL}$ and ABLH at different time-period of the day are depicted in Figure 6. Since the AOD_{ABL} is related to the ABLH, then there is more aerosol load within the ABL, as compared to the free troposphere, and thus a positive-correlation of AOD and ABLH can be observed for all files (compare Figure 5 and 6). A relatively high correlation coefficient (0.76 at 355 nm, 0.75 at 532 nm) between ABLH and AOD_{ABL} occurred in the sunrise/sunset time, while their correlation coefficients are slightly weaker (0.66 and 0.61, respectively) during the nocturnal time (residual layer effect), when aerosol load within ABL basically remain stable, due to much weaker vertical mixing at night.

The mean $ÅE_{ABL}$ is 1.54±0.37, indicating the domination of relatively small particles in the observation period. No obvious relation between $ÅE_{ABL}$ and ABLH is obtained, but higher values were observed for night time only ($ÅE_{ABL}$ > 2), i.e. more pollution emitted or less humidity. This may be partly attributed to higher number of $PM_{2.5}$ emitted during the nocturnal time (16.75±6.86 μg/m^3), as compared to the other periods (15.74±7.24μg/m^3 in the sunrise and 10.94±4.13 μg/m^3 in the sunset time). Note that given standard deviations indicate high variability of the obtained values.

Figure 7 illustrates the relations between the ABLH, PM and FCMR. Some negative trend for at well mixed layer between FCMR with ABLH can be observed, which is may suggest an increase of coarse particles (number or/and size) at the surface with an ascending ABLH. It cannot be excluded that, adiabatic effects have partly influence on the growth of particle size. Schäfer et al. (2006) found a high negative correlation between PM_{10} and ABLH in Hanover and Munich in winter. Rost et al. (2009) reported a strong negative relation between PM_{10} and ABLH in Stuttgart. Similarly, Du et al. (2013) find that $PM_{2.5}$ and ABLH exhibit negative correlation in Delhi and Xi'an. Geiß et al. (2017) reported that the link between the PM and ABLH can be attributed to several different reasons, such as meteorological conditions, terrain, local particle sources and even to the method of the ABLH retrieval itself. This was also confirmed for Warsaw by studies of long-range transported aerosol injections into the boundary layer by Stachlewska et al. (2017b, 2018). However, in general, no pronounced relationship between the PM and ABLH are

expected for Warsaw, as in Zawadzka et al. (2013). Also in the current study, no significant link between particulate matter (PM_{10} and $PM_{2.5}$) and ABLH was found for Warsaw during summer and early-autumn (Figure7), which at least partly can attributed to relatively low records of PM emissions (hourly values < 60 µg/m^3) and relatively high summer ABLHs (up to 1.6 km, Table 2). The highest PM_{10} and $PM_{2.5}$ are observed at night (NL/RL), lower at MTL, lowest at WML. Reizer et al. (2015) reported that either regional background pollution or local emission sources are mainly responsible for the high PM concentrations in Polish urban areas observed values were not high. Clearly, the ABLH is not the main factor controlling the surface pollution in summer in Warsaw, which is consistent with the reports by Bonn et al. (2016), Stachlewska et al. (2017b, 2018), and Geiß et al. (2017).

4.2 Interrelations within optical properties and with surface PM

The relations of air pollution and aerosol optical properties are given in Figures 8. The separation thresholds are defined as FCMR > 1.5 (vertical line) means that fine particles (<2.5µm) dominated and FCMR < 0.5 (vertical dashed line) means domination of coarse particles (2.5-10µm). The ÅE roughly indicates dominating particle size distribution mode, with separation thresholds of for small particles ÅE > 1.5 (horizontal line) and large particles ÅE < 1 (horizontal dashed line). However, relation between ÅE and aerosol size distribution is complicated, and so it is for the FCMR.

Figure 8 presents the relationship of AOD_{ABL}, $ÅE_{ABL}$, LR_{ABL}, δ_{ABL} and surface FCMR for the nocturnal time and transition time during July, August and September in 2013, 2015 and 2016. In general, for all time periods the values of FCMR between 0.5 and 1.5 constitute the largest proportion in total. In nocturnal time there is more fine particles than at sunset (WML), while at sunrise there is the least of fine particles. There is clear separation mark at FCMR of 1.6. There is no correlation of $ÅE_{ABL}$ and FCMR. For $1 < ÅE_{ABL} < 2$ in nocturnal time, this indicates more $PM_{2.5}$ at sunrise more PM_{10} at the surface.

Because of a weak vertical air motion (no convective mixing) and lower ABLH during the nighttime, relatively large aerosol particles are deposited in ABL and most of small aerosol particles stack below the inversion of boundary layer top (or residual layer). This should lead to an increase of number of small particles accumulated within nocturnal ABL, which manifest as fine particles increase at surface. In general, urban pollution, regarded as road traffic, industrial emission and chemical reaction of gases (SO_2, NO_2, NO_x), causes increase of both PM_{10} and $PM_{2.5}$ (He et al., 2008). The sunrise time in July-Septeber (5:00-9:00 local time) corresponds to urban traffic emission, which can cause lifting of coarse particles from the ground, thus larger amounts of coarse particles can manifest (Zawadzka et al., 2013). The relationship of LR_{ABL} and FCMR in Figure 8, shows clear separation of data, being mainly a result of higher abundance of the fine particles at MTL. On the contrary, more coarse particles (PM_{10} with higher LR_{ABL} of 40-80 sr) occur at WML.

The relationship of δ_{ABL} and FCMR in Figure 8, indicates possible negative trend (stronger at 532 nm) for all time periods. The higher the abundance of fine particles at the surface, the more spherical particles within the ABL and/or the more isotropic the atmosphere. Opposite holds for the increase of coarse particles.

Bennouna et al. (2016), reported that a significant positive correlation of PM_{10} and AOD_{CL} and increasing correlation coefficient for daily, monthly and yearly averages, relays on the aerosol characteristics of the site. Zawadzka et al. (2013), reported a negative

correlation between PM_{10} and AOD_{CL} for long-term monthly mean values in winter in Belsk and Warsaw, and a positive relation for unstable (meaning strong turbulent vertical mixing in summer) atmospheric condition in Warsaw. Relation between optical properties and surface aerosol mass concentration depends on boundary layer processes, chemical composition, source regions, weather conditions and aerosol type, which is challenging to be characterized well by columnar AOD_{ABL} and surface PM_{10} mass concentrations alone, depicted in Figure 8, AOD_{ABL} and FCMR indicates higher AOD_{ABL} for coarse particles (PM_{10}) at WML and lower for fine particles ($PM_{2.5}$) at MTL is depicted. However, no significantly correlation relation of AOD_{ABL} with PM_{10} or $PM_{2.5}$ are reported in current study. Stachlewska et al. (2018) discussed such daily mean surface PM_{10} and $PM_{2.5}$ increase with increase of the AOD_{ABL} for growing ABLH in August 2016 in Warsaw.

The significant correlations (R> 0.5) of AOD_{CL} and $PM_{2.5}$ were reported mainly for eastern cities of China (Guo et al., 2009, Zheng et al., 2015, Zang et al., 2017) and United State (Liu et al., 2007, Hutchison et al., 2008, Wang et al., 2003), where are major industrial regions with extremely pollution. In those cases, the majority of aerosol was expected to be present within boundary layer. The anthropogenic pollution in Warsaw is much lower if compared to the above mentioned regions, Zawadzka et al., 2013 reported on R=0.42 between AOD_{CL} and $PM_{2.5}$ in Warsaw, which was explained as due to significant load in free troposphere affecting this relation. The current study shows that also for AOD_{ABL} and $PM_{2.5}$ there is no significant correlation, which can be explained by low values of AOD_{ABL} and $PM_{2.5}$ were measured during investigated period due to lack of high pollution events in summer and early autumn in Warsaw. Note that in cited work Stachlewska et al., 2017b, 2018 showed AOD_{ABL} and $PM_{2.5}$ in Warsaw can be correlated, under high aerosol load conditions during events of long-range transported pollution or biomass burning injection into the boundary layers.

Similar tendency was reported by Filip & Stefan, 2011), no significant linear correlation for the nocturnal time, while some positive correlation was observed for the sunrise/sunset time (similar reported by Zawadzka et al., 2013). The ABL in summer is primarily driven by intensive convective mixing; resulting in significantly higher ABLH than in other seasons (Wang et al., 2018). In summer, the ABL aerosol can be elevated by effective convection to the free troposphere, and thus lead to decrease of aerosol loading within ABL, as reported by e.g. He et al. 2008, Tian et al. 2017. The emission of PM_{10} in summer is lower than for the other seasons in Warsaw (Zawadzka et al. 2013). Even less urban emissions at night reduce the mass concentrations of surface PM_{10}, and at the same time the aerosol properties within ABL are relatively stable due to stable boundary layer in nighttime. Therefore, no apparent relationship can be observed in nocturnal time.

Interrelations of optical properties within ABL are given in Figure 9. A positive correlation of AOD_{ABL} and LR_{ABL} is observed for all times being higher for sunrise MTL (0.64-0.72) and lower for nocturnal time (~0.56). The AOD_{ABL} and LR_{ABL} depend on extinction coefficient derived within the ABL, thus both values will increase when fine particle contribution increases and/or when there is an increase of the light absorption capability of the particles within the ABL, and vice versa. This result may be partly due to the presence of biomass burning particles inside the ABL, as e.g. in Stachlewska et al. (2018).

The relation between $ÅE_{ABL}$ and LR_{ABL} shows weak negative trend during the analysed measurement period, maybe owe to larger size particles being injected into the ABL, particles growing in the ABL or indicate smoke contribution in composition of ABL aerosol. As for the latter, a possible explanation could be that the aging smoke could have been present in the ABL, which would

be in agreement with literature, e.g. correlations of -0.79 and -0.84 between LR_{ABL} and $ÅE_{ABL}$ found for smoke particles e.g. by Giannakaki et al. (2010) and Amiridis et al. (2009). Also, Stachlewska et al. (2018) showed negative correlation of $ÅE_{ABL}$ and LR_{ABL} for smoke particles. Another explanation could be as due to the condensation of large organic molecules and particle coagulation from upper atmosphere into the ABL, as reported by e.g. Posfai et al. 2004 and Fiebig et al 2003. Giannakaki et al. (2010) showed no significant correlation of $ÅE_{ABL}$ and LR_{ABL} for continental and urban aerosols related with anthropogenic pollution. Mattis et al. (2004) also reported no relationship between $ÅE_{ABL}$ and LR_{ABL} when anthropogenic particles dominated in Leipzig. The obtained in current paper results suggest that during summer and early autumn in Warsaw, a mixture of local urban anthropogenic aerosol with natural source aerosol long-range transported into ABL, might be reasonable explanation for observing the $ÅE_{ABL}$ and LR_{ABL} weak negative tendency.

4.3 Relations of optical properties, surface PM and relative humidity

Relations between the near-surface relative humidity (RH) with surface PM_{10} and $PM_{2.5}$ and FCMR for entire, nocturnal and sunrise/sunset time were investigated. Additionally, nighttime relation between lidar derived water vapour mixing ratios (WV_{ABL}) and near-surface relative humidity (RH) with surface PM_{10} and $PM_{2.5}$ and FCMR as well as with lidar derived aerosol properties ($ÅE_{ABL,}$ LR_{ABL} and δ_{ABL}) were searched for.

Generally, in Figure 10, a weak positive trend of RH and is in agreement with the results of Sharma et al. 2017. The RH and FCMR exhibit positive correlation, with correlation coefficients of 0.6 for NT, 0.63 for WML and 0.71 for MTL. Zhang et al. 2015 reported that high relative humidity led to high $PM_{2.5}$ in Beijing. Li et al. (2017) showed that in summer urban environment, due to the hygroscopic effect on aerosols, an increase of relative humidity can lead to a growth of the fine particles $PM_{2.5}$, but not to a growth of PM_{10}, mainly attributed to the effects of wet scavenging under high summer rainfall. The mean relative humidity obtained in current study was highest for MTL (63±10 %) than for NL (57±12 %), lowest for WML (43±10 %). Then the small particles have greater possibility to aggregate into relatively large particles at nighttime, and thus lower correlation coefficients for RH and $PM_{2.5}$ (and FCMR) are found for the nocturnal time.

Figure 11 presents no relation of water vapour mixing ratio within WV_{ABL} with $PM_{2.5}$, PM_{10} and FCMR in nocturnal time in Warsaw. The correlation coefficient of WV_{ABL} and $PM_{2.5}$ is a little higher than WV_{ABL} and PM_{10}, indicating that water vapour in ABL affects surface fine particles more than surface coarse particles. Presence of anthropogenic particles in the ABL, as these hygroscopic particles absorb water vapour and its gradually increase in size. Furthermore, growth of particles due to coagulation of particles within ABL cannot be excluded (Fiebig et al., 2003).

Figure 11, depicts also scatter plots of water vapour mixing ratio and aerosol optical properties. No clear relations found between WV_{ABL} and AOD_{ABL}, $ÅE_{ABL}$ and LR_{ABL}. Only δ_{ABL} and WV_{ABL} show a negative trend (Figure 11). The hygroscopicity of particles increases with decreasing particle size, Petters et al. 2009. At the same time, the more fine particles the lower the depolarization (see Figure 8). Hence, increase of water vapour and presence of hygroscopic particles leads to decrease of depolarization. For occurrence of long-range transported aerosol of biomass burning, hygroscopic effects can be well captured with quasi-continuous

profiling of water vapour (Stachlewska et al., 2017a). Note that the relation of the AOD_{ABL}, $ÅE_{ABL}$ and LR_{ABL} with the surface RH also shows not much of any trend for NL, however for WML the negative trends and properties grouping becomes more visible (Figure 12).

The AOD_{CL} was reported to increase with ambient relative humidity for hygroscopic particles due to hygroscopic growth (Bergin et al., 2000, Altaratz et al., 2013). A negative relation between AOD_{ABL} and surface RH is found in the current study, except for nocturnal time in Figure 12. With high surface RH lower AOD_{ABL} is observed. The size and optical properties can change as aerosol particles uptake water and higher RH is more favorable for hygroscopic growth of pollution particles (Tang, 1996).

During observational period, the main composition within boundary layer was due to urban anthropogenic aerosols. Increase of RH leads to increasing pollution particle size, which is visible at nighttime (ÅE and RH show slight negative trend), while slight positive trend is between $ÅE_{ABL}$ and RH at transition times (different grouping in moister MTL and drier WML), being in accordance with the FCMR and ÅE scatter plots (more coarse particles in MTL and more fine particles in WML). Pollution particle within boundary layer due to weaker convective mixing at nighttime, are prone to surface water uptake which contributes to an increase of aerosol particle size Cheng et al. (2008). The relation between LR_{ABL} and RH shows practically no correlation in nocturnal time but it is well separated in transition time (lower LR for MTL). At nighttime, increasing LR due to accumulation of hygroscopic smoke particles was reported by Giannkaki et al. (2010). Convection and energy exchange is stronger in the transition time (Stull.2012), leading to anthropogenic aerosol dominated in aerosol boundary layer, increasing surface RH results in the rise of aerosol particles size, and thus contributes to decreasing LR_{ABL}. The negative trend of relation between δ_{ABL} and surface RH (nicely pronounced at nocturnal time) is in agreement with trend obtained for WV_{ABL} and δ_{ABL}.

As such, the obtained extensive data set have a potential to be used for testing and interpreting results of aerosol typing algorithms, especially those needing sets of Raman-derived lidar products as they are using artificial neural network approaches for aerosol categorization (Nicolae et al., 2018).

5 Conclusions

The study of optical properties within ABL calculated at 355 and 532 nm based on EARLINET dataset on July, August and September during 2013, 2015 and 2016 in Warsaw was conducted. Interrelations of different optical properties within ABL were discussed. In addition, an attempt to find any relations of aerosol optical properties within ABL and PM were highlighted. The comparison of various parameters was analysed in three different periods (entire time, nocturnal time and sunrise/sunset time).

AOD_{ABL} and LR_{ABL} at both wavelengths at sunrise are relatively higher than for the other two periods, indicating that convective mixing, and change of atmospheric conditions impact light extinction on aerosol particles in the ABL. In nocturnal period, $ÅE_{ABL}$ values are higher than for the two remaining periods, suggesting smaller particles dominate at nighttime during summer time in Warsaw. Aerosols composition within ABL of summer and early-autumn in Warsaw, consists of urban anthropogenic pollution, biomass burning aerosols, arctic marine particles and their mixtures. Comparison of AOD_{ABL} with columnar AOD_{CL}, found the latter twice higher when optically thick aerosol layers due to long-range transport of air-masses were observed above the ABL,

and less than 2 times higher for cases with no aerosol layers in the free troposphere (but with presence of aloft pollution due to convection). The AOD_{CL} and ABLH are tend to be negatively related, which can be attributed to the influence of smoke layers suspended in free troposphere. The AOD_{ABL} and ABLH exhibit positive correlation (~ 0.70) in observation period. There $ÅE_{ABL}$ and ABLH seem to be negatively related, while $ÅE_{ABL}$ and FCMR positively, although the latter is being far from statistical significance, still for MTL both properties are higher than for the WML). A negative-correlation of δ_{ABL} and FCMR was found for all time-periods, which indicates higher sphericity of fine particles and thus higher isotropy of the atmosphere what consisting of fine particles. Reported in literature, different correlations obtained for AOD_{ABL} and PM_{10} are explained as due to complicated atmospheric and weather conditions. In summer and early-autumn in Warsaw, there is generally high-pressure systems that govern the dynamics of the atmosphere, there is significantly less traffic pollution (people on holidays, on bicycles), pollination of plants plays role. The relation between AOD_{ABL} and FCMR reported here, displays positive correlation only at sunrise and this can be due to traffic peaks. Due to less urban emissions (neither traffic nor domestic heating) and relatively stable boundary layer at nighttime, no apparent relationship of AOD_{ABL} with FCMR was observed. The AOD_{ABL} and LR_{ABL} depend on extinction coefficient derived inside the ABL, thus their positive correlation is observed. Relation of $ÅE_{ABL}$ and LR_{ABL} reveals weak negative trend. When ABLH grows, a declining trend of FCMR is observed for WML, indicating an increase of coarse particle fraction. However, there is no clearly apparent link between PM_{10} or $PM_{2.5}$ and ABLH.

The weak positive correlation coefficient of nighttime WV_{ABL} with $PM_{2.5}$ is higher than with PM_{10}, indicating that water vapour in NL(RL) affects surface fine particles more than surface coarse particles. The increasing WV_{ABL} can lead to the decrease of depolarization due to the presence of hygroscopic particles, and the relation between near-surface and depolarization is the same. Near-surface relative humidity can decrease AOD_{ABL}, because change of aerosol particle in type and size within ABL.

A negative trend of δ_{ABL} and $WV_{ABL,}$ δ_{ABL} and RH is due to the hygroscopicity of particles increase. A negative relation between AOD_{ABL} and surface RH is found for daytime WML, which is followed by a weak negative correlation of LR_{ABL} and RH is observed only during sunset time.

The obtained results contribute to increase of knowledge on variability of optical properties within summertime aerosol boundary layer at a continental urban site in central Europe. Relations found in already published research, obtained on the basis of case-study approach, do not necessarily apply nor are seen in the long-term study. Therefore, special care should be taken when interpreting and comparing the different results.

Bottom line is that regular, automated observations with the NeXT generation PollyXT lidar conducted at the EARLINET site allow for such studies. The excellent capabilities of this lidar gave possibility to combine the derived within this preliminary study lidar results with other data sources (e.g. AERONET, WIOS, PolandAOD). Hypothesis for boundary layer aerosol properties interrelations were proposed and will be further verified with more lidar data of regular observations in Warsaw. What could be improved by enlarging the existing high-quality lidar data sample is investigation of subgrouping of aerosol properties that could provide statistically significant correlations. Further, more observations will allow for extension of search for differences to other seasons, daytime analyses, and distinguishing sunset from sunrise aerosol properties relationships. Finally, a separation of aerosol

properties accordingly to aerosol content, i.e. pure urban versus its mixture with other aerosol types, would be possible (currently too little data in mixed categories) and estimation of their radiative effect.

Acknowledgments:

This research has been done in the frame of the Technical assistance for Polish Radar and Lidar Mobile Observation System (POLIMOS) funded by ESA-ESTEC Contract no. 4000119961/16/NL/FF/mg.

The PollyXT-Warsaw lidar was developed in a scientific collaboration of the Faculty of Physics, University of Warsaw (FUW) with the Institute of Tropospheric Research (TROPOS). This development was financed by the Polish Foundation of Science and Technology (FNTP-No. 519/FNITP/115/2010). We especially acknowledge colleagues of the PollyXT Lidar Group lead by Dietrich Althausen.

Authors acknowledge the Warsaw Regional Inspectorate of Environmental Protection WIOS-Warsaw for provision of the processed $PM_{2.5}$ and PM_{10} data, visualised at http://www.wios.warszawa.pl. The data were accessed via the Data Archive of the National Chief Inspectorate for Environmental Protection (GIOS) via http://powietrze.gios.gov.pl/pjp/archive.

We acknowledge Brent Holben for processing of the AERONET data (https://AERONETl .gsfc.nasa.gov); Aleksander Pietruczuk and Piotr Sobolewski of Institute of Geophysics at Polish Academy of Sciences for performing the AERONET measurements in Belsk; Phillippe Golub for performing instrument calibrations at the PHOTONS/AERONET-EUROPE calibration center, supported by ACTRIS-1 project funded within the European Union Seventh Framework Program (FP7/2007e2013) under Grant Agreement No.262254.

We acknowledge Krzysztof Markowicz for processing of the MFR-7 data within the Polish aerosol Research Network PolandAOD-NET (https://polandaod.pl). The MFR-7 radiometer was purchased within a grant No.1283/B/P01/2010/38 of the Polish Ministry of Science and High Education.

The EARLINET is currently supported by the ACTRIS-2 project, funded by the European Union Research Infrastructure Action under the H2020 specific program for Integrating and opening existing national and regional research infrastructures of European interest under Grant Agreement No. 654109 and No. 739530. The University of Warsaw participates in ACTRIS-2 project as an associate partner without funding.

Author Contributions:

I.S.Stachlewska wrote the paper, obtained funding for the research, came up with the study approach, designed methodology, and performed experiment, contributed to development of PollyXT-Warsaw lidar and lidar evaluation algorithms, took care of quality assurance of lidar measurements and data products, and holistically interpreted the lidar results with other data sources results (AERONET, PolandAOD-NET, WIOS Monitoring Network). D.Szczepanik contributed with calculation of the aerosol optical properties profiles (α, β, δ) and with their categorization for the EARLINET/ACTRIS Data Base. D.Wang contributed with extensive literature review, wrote the codes for the ABLH and the WV retrieval algorithms, and performed statistical analysis of the optical properties (AE, LR, δ, WV). All authors contributed with merit revisions of the paper.

Conflicts of Interest: The authors declare no conflict of interest.

Appendix: Lists of symbols and physical quantities:

Entire time	-- ET
Nocturnal time	-- NT
Transition rime	-- TT
Aerosol boundary layer (derived by lidar)	-- ABL
Aerosol boundary layer height (derived by lidar)	-- ABLH
Residual layer (derived by lidar)	-- RL
Nocturnal layer (derived by lidar)	-- NL
Morning transition layer (derived by lidar)	-- MTL
Well mixed layer (derived by lidar)	-- WML
Particle extinction coefficient (within aerosol boundary layer)	-- α_{ABL}
Particle backscatter coefficient (within aerosol boundary layer)	-- β_{ABL}
Aerosol optical depth (within aerosol boundary layer, derived by lidar)	-- $AOD_{ABL}(\lambda)$
Aerosol optical depth (columnar, derived by sun-photometer or radiometer)	-- $AOD_{CL}(\lambda)$
Lidar ratio (within aerosol boundary layer)	-- $LR_{ABL}(\lambda)$
Particle linear depolarization ratio (within aerosol boundary layer)	-- $\delta_{ABL}(\lambda)$
Ångstrom exponent (within aerosol boundary layer, derived by lidar)	-- $ÅE_{ABL}(\lambda_1/\lambda_2)$
Ångstrom exponent (columnar, derived by sun-photometer or radiometer)	-- $ÅE_{CL}(\lambda_1/\lambda_2)$
Water vapor mixing ratio (within aerosol boundary layer)	-- WV_{ABL}
Relative humidity (at the near-surface)	-- RH
Particulate matter with diameter <10 μm; <2.5 μm	-- PM_{10}; $PM_{2.5}$
Fine to coarse mass ratio	-- FCMR
Wavelength	-- λ

References

Angstrom, A.: On the atmospheric transmission of sun radiation and on dust in the air, Geogr. Ann., 12, 156–166, https://doi.org/10.1080/20014422.1929.11880498, 1929**.**

Altaratz, O., Bar-Or, R. Z., Wollner, U., and Koren, I.: Relative humidity and its effect on aerosol optical depth in the vicinity of convective clouds, Environ. Res. Lett., 8, 034025, https://doi.org/10.1088/1748-9326/8/3/034025, 2013.

Alados-Arboledas, L., Müller, D., Guerrero-Rascado, J., Navas-Guzmán, F., Pérez-Ramírez, D., and Olmo, F.: Optical and microphysical properties of fresh biomass burning aerosol retrieved by Raman lidar, and star-and sun- photometry, Geophys. Res. Lett., 38, https://doi.org/10.1029/2010GL045999, 2011.

Alastuey, A., Querol, X., Castillo, S., Escudero, M., Avila, A., Cuevas, E., Torres, C., Romero, P. M., Exposito, F., and García, O.: Characterisation of TSP and $PM_{2.5}$ at Izaña and Sta. Cruz de Tenerife (Canary Islands, Spain) during a Saharan Dust Episode (July 2002), Atmos. Environ., 39, 4715-4728, https://doi.org/10.1016/j.atmosenv.2005.04.018, 2005.

Amiridis, V., Balis, D., Kazadzis, S., Bais, A., Giannakaki, E., Papayannis, A., and Zerefos, C.: Four-year aerosol observations with a Raman lidar at Thessaloniki, Greece, in the framework of European Aerosol Research Lidar Network (EARLINET), J. Geophys. Res., 110, https://doi.org/10.1029/2005JD006190, 2005.

Amiridis, V., Balis, D., Giannakaki, E., Stohl, A., Kazadzis, S., Koukouli, M., and Zanis, P.: Optical characteristics of biomass burning aerosols over Southeastern Europe determined from UV-Raman lidar measurements, Atmos. Chem. Phys., 9, 2431-2440, https://doi.org/10.5194/acp-9-2431-2009, 2009.

Ansmann, A., Tesche, M., Knippertz, P., Bierwirth, E., Althausen, D., Mueller, D., and Schulz, O.: Vertical profiling of convective dust plumes in Southern Morocco during SAMUM, Tellus B: Chem. and Phys. Meteo., 61, 340-353, https://doi.org/10.1111/j.1600-0889.2008.00384.x, 2009.

Ansmann, A., Baars, H., Chudnovsky, A., Mattis, I., Veselovskii, I., Haarig, M., Seifert, P., Engelmann, R., and Wandinger, U.: Extreme levels of Canadian wildfire smoke in the stratosphere over Central Europe on 21–22 August 2017, Atmos. Chem. Phys., 18, 11831-11845, https://doi.org/10.5194/acp-18-118312018, 2018.

Baars, H., Kanitz, T., Engelmann, R., Althausen, D., Heese, B., Komppula, M., Preißler, J., Tesche, M., Ansmann, A., Wandinger, U, Lim, J.-H., Ahn, J. Y., Stachlewska, I. S., Amiridis, V., Marinou, E., Seifert, P., Hofer, J., Skupin, A., Schneider, F., Bohlmann, S., Foth, A., Bley, S., Pfüller, A., Giannakaki, E., Lihavainen, H., Viisanen, Y., Hooda, R. K., Pereira, S. N., Bortoli, D., Wagner, F., Mattis, I., Janicka, L., Markowicz, K. M., Achtert, P., Artaxo, P., Pauliquevis, T., Souza, R. A. F., Sharma, V. P., van Zyl, P. G., Beukes, J. P., Sun, J., Rohwer, E. G., Deng, R., Mamouri, R.-E., and Zamorano, F.: An overview of the first decade of Polly^{NET}: An emerging network of automated Raman-polarization lidars for continuous aerosol profiling, Atmos. Chem. Phys., 16, 5111-5137, https://doi.org/10.5194/acp-16-5111-2016, 2016.

Barlage, M., Miao, S., and Chen, F.: Impact of physics parameterizations on high-resolution weather prediction over two Chinese megacities, J. Geophys. Res., 121, 4487-4498, https://doi.org/10.1002/2015JD024450, 2016.

Bennouna, Y., Cachorro, V. E., Mateos, D., Burgos, M. A., Toledano, C., Torres, B., and de Frutos, A.: Long-term comparative study of columnar and surface mass concentration aerosol properties in a background environment, Atmos. Environ., 140, 261-272, https://doi.org/10.1016/j.atmosenv.2016.05.061, 2016.

Bonn, B., von Schneidemesser, E., Andrich, D., Quedenau, J., Gerwig, H., Lüdecke, A., Kura, J., Pietsch, A., Ehlers, C., Klemp, D., Kofahl, C., Nothard, R., Kerschbaumer, A., Junkermann, W., Grote, R., Pohl, T., Weber, K., Lode, B., Schönberger, P., Churkina, G., Butler, T. M., and Lawrence, M. G.: BAERLIN2014 – the influence of land surface types

on and the horizontal heterogeneity of air pollutant levels in Berlin, Atmos. Chem. Phys., 16, 7785-7811, https://doi.org/10.5194/acp-16-7785-2016, 2016.

Böckmann, C., Wandinger, U., Ansmann, A., Bösenberg, J., Amiridis, V., Boselli, A., Delaval, A., De Tomasi, F., Frioud, M., and Grigorov, I. V.: Aerosol lidar intercomparison in the framework of the EARLINET project. 2. Aerosol backscatter algorithms, Appl. Opt., 43, 977-989, https://doi.org/10.1364/AO.43.000977, 2004.

Burton, S. P., Ferrare, R. A., Hostetler, C. A., Hair, J. W., Rogers, R. R., Obland, M. D., Butler, C. F., Cook, A. L., Harper, D. B., and Froyd, K. D.: Aerosol classification using airborne High Spectral Resolution Lidar measurements–methodology and examples, Atmos. Meas. Tech., 5, 73-98, https://doi.org/10.5194/amt-5-73-2012, 2012.

Bergin, M. H., Schwartz, S. E., Halthore, R. N., Ogren, J. A., and Hlavka, D. L.: Comparison of aerosol optical depth inferred from surface measurements with that determined by Sun photometry for cloud-free conditions at a continental US site, J. Geophys. Res., 105, 6807–6816, https://doi.org/10.1029/1999JD900454, 2000.

Béghein C., Allery C., Wacławczyk C., and Pozorski J.: Application of POD-based dynamical systems to dispersion and deposition of particles in turbulent channel flow, Int. J. Multiphase Flow, 58, 97-113, https://doi.org/10.1016/j.ijmultiphaseflow .2013.09.001, 2014.

Cheng, Y. F., Wiedensohler, A., Eichler, H., Heintzenberg, J., Tesche, M., Ansmann, A., Wendisch, M., Su, H., Althausen, D., Herrmann, H., Gnauk, T., Brüggemann, E., Hu, M., and Zhang, Y. H.: Relative humidity dependence of aerosol optical properties and direct radiative forcing in the surface boundary layer at Xinken in Pearl River Delta of China: An observation based numerical study, Atmos. Environ., 42, 6373–6397, https://doi.org/10.1016/j.atmosenv.2008.04.009, 2008.

Chen, B., and Kan, H.: Air pollution and population health: A global challenge, Environ. Health Prev. Med., 13, 94-101, https://doi.org/10.1007/s12199-007-0018-5, 2008.

Chilinski, M. T., Markowicz, K. M., Zawadzka, O., Stachlewska, I. S., Kumala, W., Petelski, T., Makuch, P., Westphal, D. L., and Zagajewski, B.: Modelling and Observation of Mineral Dust Optical Properties over Central Europe, Acta Geophys., 64 (6), 2550-2590, https://doi:10.1515/acgeo-2016-0069, 2016.

Costa-Surós, M., Stachlewska, I. S., Nemuc, A., Talianu, C., Heese, B., and Engelmann, R.: Study case of air-mass modification over Poland and Romania observed by the means of multiwavelength Raman depolarization lidars, the 27th International Laser Radar Conference, New York, USA, 5-10 July 2015, 1-4, 2015.

Dawson, K. W., Meskhidze, N., Josset, D., and Gassó, S.: Spaceborne observations of the lidar ratio of marine aerosols, Atmos. Chem. Phys., 15, 3241-3255, https://doi.org/10.5194/acp-15-3241-2015, 2015.

De Leeuw, F., Sluyter, R., van Breugel, P., and Bogman, F.: Air Pollution by ozone in Europe in 1999 and the summer of 2000, European Environmental Agency Topic Report number 1/2001, EEA, Copenhagen, Denmark, 2001.

Du, C., Liu, S., Yu, X., Li, X., Chen, C., Peng, Y., Dong, Y., Dong, Z., and Wang, F.: Urban boundary layer height characteristics and relationship with particulate matter mass concentrations in Xi'an, Central China, aerosol, Air Qual. Res., 13, 1598-1607, https://doi:10.4209/aaqr.2012.10.0274, 2013.

Engelmann, R., Kanitz, T., Baars, H., Heese, B., Althausen, D., Skupin, A., Wandinger, U., Komppula, M., Stachlewska, I.S., Amiridis, V, Marinou, E., Mattis, I., Linné, H., and Ansmann, A.: The automated multiwavelength Raman polarization and water-vapor lidar Polly^{XT}: The neXT generation, Atmos. Meas. Tech., 9, 1767-1784, https://doi.org/10.5194/amt-9-1767-2016, 2016.

Fiebig, M., Stohl, A., Wendisch, M., Eckhardt, S., and Petzold, A.: Dependence of solar radiative forcing of forest fire aerosol on ageing and state of mixture, Atmos. Chem. Phys., 3, 881-891, https://doi.org/10.5194/acp-3-881-2003, 2003.

Filip, L. and Stefan, S.: Study of the correlation between the near-ground PM10 mass concentration and the aerosol optical depth. J. Atmos. Solar.-Terrestrial. Phys., 73, 1883-1889, https://doi.org/10.1016/j.jastp.2011.04.027, 2011.

Flentje, H., Heese, B., Reichardt, J., and Thomas, W.: Aerosol profiling using the ceilometer network of the German Meteorological Service, Atmos. Meas. Tech. Discuss., 3, 3643-3673, https://doi.org/10.5194/amtd-3-3643-2010, 2010.

Freudenthaler, V., Esselborn, M., Wiegner, M., Heese, B., Tesche, M., Ansmann, A., Müller, D., Althausen, D., Wirth, M., Fix, A., Ehret, G., Knippertz, P., Toledano, C., Gasteiger, J., Garhammer, M., and Seefeldner, M.: Depolarization ratio profiling at several wavelengths in pure Saharan dust during SAMUM 2006, Tellus B, 61, 165–179, https://doi:10.1111/j.1600-0889.2008.00396.x, 2009.

Freudenthaler, V., Linné, H., Chaikovski, A., Rabus, D., and Groß, S.: EARLINET lidar quality assurance tools, Atmos. Meas. Tech. Discuss., https://doi.org/10.5194/amt-2017-395, in review, 2018.

Gasteiger, J., and Freudenthaler, V.: Benefit of depolarization ratio at λ=1064 nm for the retrieval of the aerosol microphysics from lidar measurements, Atmos. Meas. Tech., 7, 3773-3781, https://doi.org/10.5194/amt-7-3773-2014, 2014.

Groß, S., Tesche, M., Freudenthaler, V., Toledano, C., Wiegner, M., Ansmann, A., Althausen, D., and Seefeldner, M.: Characterization of Saharan dust, marine aerosols and mixtures of biomass-burning aerosols and dust by means of multi-wavelength depolarization and Raman lidar measurements during SAMUM 2, Tellus B: Chem. and Phys. Meteo., 63, 706-724, https://doi.org/10.1111/j.1600-0889.2011.00556.x, 2011.

Groß, S., Esselborn, M., Weinzierl, B., Wirth, M., Fix, A., and Petzold, A.: Aerosol classification by airborne high spectral resolution lidar observations, Atmos. Chem. Phys., 13, 2487–2505, https://doi:10.5194/acp-13-2487-2013, 2013.

Groß, S., Freudenthaler, V., Schepanski, K., Toledano, C., Schäfler, A., Ansmann, A., and Weinzierl, B.: Optical properties of long-range transported Saharan dust over Barbados as measured by dual-wavelength depolarization Raman lidar measurements, Atmos. Chem. Phys., 15, 11067–11080, https://doi.org/10.5194/acp-15-11067-2015, 2015.

Geiß, A., Wiegner, M., Bonn, B., Schäfer, K., Forkel, R., von Schneidemesser, E., Münkel, C., Chan, K. L., and Nothard, R.: Mixing layer height as an indicator for urban air quality?, Atmos. Meas. Tech., 10, 2969-2988, https://doi.org/10.5194/amt-10-2969-2017, 2017.

Giannakaki, E., Balis, D., Amiridis, V., and Zerefos, C.: Optical properties of different aerosol types: Seven years of combined Raman-elastic backscatter lidar measurements in Thessaloniki, Greece, Atmos. Meas. Tech., 3, 569-578, https://doi.org/10.5194/amt-3-569-2010, 2010.

Guo, J.-P., Zhang, X.-Y., Che, H.-Z., Gong, S.-L., An, X., Cao, C.-X., Guang, J., Zhang, H., Wang, Y.-Q., Zhang, X.-C., Xue, M., and Li, X.-W.: Correlation between PM concentrations and aerosol optical depth in eastern China, Atmos. Environ., 43, 5876–5886, https://doi.org/10.1016/j.atmosenv.2009.08.026, 2009.

Guo, H., Wang, Y., and Zhang, H.: Characterization of criteria air pollutants in Beijing during 2014–2015. Environ. Res., 154, 334-344, https://doi.org/10.1016/j.envres.2017.01.029, 2017.

Haarig, M., Ansmann, A., Gasteiger, J., Kandler, K., Althausen, D., Baars, H., Radenz, M., and Farrell, D. A.: Dry versus wet marine particle optical properties: RH dependence of depolarization ratio, backscatter, and extinction from multiwavelength lidar measurements during SALTRACE, Atmos. Chem. Phys., 17, 14199-14217, https://doi.org/10.5194/acp-17-14199-2017, 2017.

Haarig, M., Ansmann, A., Baars, H., Jimenez, C., Veselovskii, I., Engelmann, R., and Althausen, D.: Depolarization and lidar ratios at 355, 532, and 1064 nm and microphysical properties of aged tropospheric and stratospheric Canadian wildfire smoke, Atmos. Chem. Phys., 18, 11847-11861, https://doi.org/10.5194/acp-18-11847-2018, 2018.

Harrison, L., Michalsky, J., and Berndt, J.: Automated multifilter rotating shadow-band radiometer: An instrument for optical depth and radiation measurements, Appl. Opt., 33, 5118-5125, https://doi.org/10.1364/AO.33.005118, 1994.

Hutchison, K. D., Faruqui, S. J., and Smith, S.: Improving correlations between MODIS aerosol optical thickness and ground-based PM2.5 observations through 3D spatial analyses, Atmos. Environ., 42, 530–543, https://doi.org/10.1016/j.atmosenv.2007.09.050, 2008.

Hu, Q., Goloub, P., Veselovskii, I., Bravo-Aranda, J.-A., Popovici, I. E., Podvin, T., Haeffelin, M., Lopatin, A., Dubovik, O., Pietras, C., Huang, X., Torres, B., and Chen, C.: Long-range-transported Canadian smoke plumes in the lower stratosphere over northern France, Atmos. Chem. Phys., 19, 1173-1193, https://doi.org/10.5194/acp-19-1173-2019, 2019.

He, Q., Li, C., Mao, J., Lau, A. K. H., and Chu, D.: Analysis of aerosol vertical distribution and variability in Hong Kong, J. Geophys. Res., 113, https://doi.org/10.1029/2008JD009778, 2008.

Heese, B., and Wiegner, M.: Vertical aerosol profiles from Raman polarization lidar observations during the dry season AMMA field campaign, J. Geophys. Res., 113, https://doi.org/10.1029/2007JD009487, 2008.

Holben, B. N., Eck, T. F., Slutsker, I., Tanre, D., Buis, J. P., Setzer, A., Vermote, E., Reagan, J. A., Kaufman, Y. J., Nakjima, T., Lavenu, F., Jankowiak, I., and Smirnov, A.: AERONE – A federated instrument network and data archive for aerosol characterization, Remote Sens. Environ., 66, 1–16, https://doi.org/10.1016/S0034-4257(98)00031-5, 1998.

Iqbal, M.: An introduction to solar radiation, Acadamec Press, Ontario, 1983.

Janicka, L., Stachlewska, I. S., Veselovskii, I., and Baars, H.: Temporal variations in optical and microphysical properties of mineral dust and biomass burning aerosol derived from daytime Raman lidar observations over Warsaw, Poland, Atmos. Environ., 169, 162-174, https://doi.org/10.1016/j.atmosenv.2017.09.022, 2017.

Janicka, L. and Stachlewska, I. S.: Properties of biomass burning aerosol mixtures derived at fine temporal and spatial scales from Raman lidar measurements: Part I optical properties, Atmos. Chem. Phys. Discuss., https://doi.org/10.5194/acp-2019-207, in review, 2019.

Juda-Rezler K., Reizer, M., and Oudinet, J.P.: Determination and analysis of PM10 source apportionment during episodes of air pollution in Central Eastern European urban areas: The case of wintertime 2006, Atmos. Environ., 45(36), 6557-6566, https://doi.org/10.1016/j.atmosenv.2011.08.020, 2011.

Juda-Rezler, K., Reizer, M., Huszar, P., Krueger, B., Zanis, P., Syrakov, D., Katragkou, E., Trapp, W., Melas, D., Chervenkov, H., Tegoulias, I., and Halenka, T.: Modelling the effects of climate change on air quality over central and Eastern Europe: concept, evaluation and projections, Clim. Res., 53, 179–203, https://doi.org/10.3354/cr01072, 2012.

Kaufman, Y. J., Tanré, D., and Boucher, O.: A satellite view of aerosols in the climate system, Nature, 419, 215, https://doi.org/10.1038/nature01091, 2002.

Lelieveld, J., Evans, J. S., Fnais, M., Giannadaki, D., and Pozzer, A.: The contribution of outdoor air pollution sources to premature mortality on a global scale, Nature, 525, 367, https://doi.org/10.1038/nature15371, 2015.

Li, X., Ma, Y., Wang, Y., Liu, N., and Hong, Y.: Temporal and spatial analyses of particulate matter (PM10 and PM2. 5) and its relationship with meteorological parameters over an urban city in Northeast China, Atmos. Res., 198, 185-193, https://doi.org/10.1016/j.atmosres.2017.08.023, 2017.

Liu, Y., Franklin, M., Kahn, R., and Koutrakis, P.: Using aerosol optical thickness to predict ground-level PM2.5 concentrations in the St. Louis area: A comparison between MISR and MODIS, Remote Sens. Environ., 107, 33–44, https://doi.org/10.1016/j.rse.2006.05.022, 2007.

Marinou, E., Amiridis, V., Binietoglou, I., Tsikerdekis, A., Solomos, S., Proestakis, E., Konsta D., Papagiannopoulos, N., Tsekeri, A., and Vlastou, G.: Three-dimensional evolution of Saharan dust transport towards Europe based on a 9-year EARLINET-optimized CALIPSO dataset, Atmos. Chem. Phys., 17, https://doi.org/10.5194/acp-17-5893-2017, 2017.

Markowicz, K., Chilinski, M.T., Lisok, J., Zawadzka, O., Stachlewska, I.S., Janicka, L., Rozwadowska, A., Makuch, P., Pakszys, P., Zielinski, T., Petelski, T., Posyniak, M., Pietruczuk, A., Szkop, A., and Westphal, D.L.: Study of aerosol optical properties during long-range transport of biomass burning from Canada to Central Europe in July 2013, J. Aeros. Sci., 101, 156-173, https://doi.org/10.1016/j.jaerosci.2016.08.006, 2016.

Masonis, S. J., Anderson, T. L., Covert, D. S., Kapustin, V., Clarke, A. D., Howell, S., and Moore, K.: A study of the extinction-to-backscatter ratio of marine aerosol during the shoreline environment aerosol study, J. Atmos. Ocean. Techn., 20, 1388-1402, https://doi.org/10.1175/1520-0426(2003)020<1388:ASOTER>2.0.CO;2, 2003.

Matthias, V., Balis, D., Bösenberg, J., Eixmann, R., Iarlori, M., Komguem, L., Mattis, I., Papayannis, A., Pappalardo, G., and Perrone, M.: Vertical aerosol distribution over Europe: Statistical analysis of Raman lidar data from 10 European aerosol research lidar network (EARLINET) stations, J. Geophys. Res., 109, https://doi.org/10.1029/2004JD004638, 2004.

Mattis, I., Ansmann, A., Müller, D., Wandinger, U., and Althausen, D.: Multiyear aerosol observations with dual-wavelength Raman lidar in the framework of EARLINET, J. Geophys. Res., 109, https://doi.org/10.1029/2004JD004600, 2004.

Müller, D., Ansmann, A., Mattis, I., Tesche, M., Wandinger, U., Althausen, D., and Pisani, G.: Aerosol-type-dependent lidar ratios observed with Raman lidar, J. Geophys. Res., 112, https://doi.org/10.1029/2006JD008292, 2007.

Navas Guzmán, F., Martucci, G., Collaud Coen, M., Granados Muñoz, M. J., Hervo, M., Sicard, M., and Haefele, A.: Towards continuous monitoring of aerosol hygroscopicity by Raman lidar measurements at the EARLINET station of Payerne, Atmos. Chem. Phys. Discuss., https://doi.org/10.5194/acp-2019-289, in review, 2019.

Nicolae, D., Vasilescu, J., Talianu, C., Binietoglou, I., Nicolae, V., Andrei, S., and Antonescu, B.: A neural network aerosol-typing algorithm based on lidar data, Atmos. Chem. Phys., 18, 14511-14537, https://doi.org/10.5194/acp-18-14511-2018, 2018.

Nemuc, A., Vasilescu, J., Talianu, C., Belegante, L., and Nicolae, D.: Assessment of aerosol's mass concentrations from measured linear particle depolarization ratio (vertically resolved) and simulations, Atmos. Meas. Tech., 6, 3243-3255, https://doi.org/10.5194/amt-6-3243-2013, 2013.

Ortiz-Amezcua, P., Guerrero-Rascado, J. L., Granados-Muñoz, M. J., Benavent-Oltra, J. A., Böckmann, C., Samaras, S., Stachlewska, I. S., Janicka, Ł., Baars, H., and Bohlmann, S.: Microphysical characterization of long-range transported biomass burning particles from North America at three EARLINET stations, Atmos. Chem. Phys., 17, 5931-5946, https://doi.org/10.5194/acp-17-5931-2017, 2017.

Pandolfi, M., Martucci, G., Querol, X., Alastuey, A., Wilsenack, F., Frey, S., O'Dowd, C., and Dall'Osto, M.: Continuous aerosol boundary layer observations in the coastal urban area of Barcelona during SAPUSS, Atmos. Chem. Phys., 13, 4983-4996, https://doi.org/10.5194/acp-13-4983-2013, 2013.

Papagiannopoulos, N., Mona, L., Amodeo, A., D'Amico, G., Gumà Claramunt, P., Pappalardo, G., Alados-Arboledas, L., Guerrero-Rascado, J. L., Amiridis, V., Kokkalis, P., Apituley, A., Baars, H., Schwarz, A., Wandinger, U., Binietoglou, I., Nicolae, D., Bortoli, D., Comerón, A., Rodríguez-Gómez, A., Sicard, M., Papayannis, A., and Wiegner, M.: An automatic observation-based aerosol typing method for EARLINET, Atmos. Chem. Phys., 18, 15879-15901, https://doi.org/10.5194/acp-18-15879-2018, 2018.

Papayannis, A., Amiridis, V., Mona, L., Tsaknakis, G., Balis, D., Bosenberg, J., Chaikovski, A., De Tomasi, F., Grigorov, I., Mattis, I., Mitev, V., Muller, D., Nickovic, S., Perez, C., Pietruczuk, A., Pisani, G., Ravetta, F., Rizi, V., Sicard, M., Trickl, T., Wiegner, M., Gerding, M., Mamouri, R. E., D'Amico, G., and Pappalardo, G.: Systematic lidar observations of Saharan dust over Europe in the frame of EARLINET (2000–2002), J. Geophys. Res., 113, D10204, https://doi.org/10.1029/2007JD009028, 2008.

Pappalardo, G., Amodeo, A., Apituley, A., Comeron, A., Freudenthaler, V., Linné, H., Ansmann, A., Bösenberg, J., D'Amico, G., and Mattis, I.: EARLINET: Towards an advanced sustainable European aerosol lidar network, Atmos. Meas. Tech., 7, 2389-2409, https://doi.org/10.5194/amt-7-2389-2014, 2014.

Pérez, C., Sicard, M., Jorba, O., Comerón, A., and Baldasano, J.M.: Summertime re-circulations of air pollutants over the north-eastern Iberian coast observed from systematic EARLINET lidar measurements in Barcelona, Atmos. Environ., 38, 3983-4000, https://doi.org/10.1016/j.atmosenv.2004.04.010, 2004.

Perrone, M. R., De Tomasi, F., and Gobbi, G. P.: Vertically resolved aerosol properties by multi-wavelength lidar measurements, Atmos. Chem. Phys., 14, 1185-1204, https://doi.org/10.5194/acp-14-1185-2014, 2014.

Petters, M. D., Carrico, C. M., Kreidenweis, S. M., Prenni, A. J., DeMott, P. J., Collett, J. L., and Moosmüller, H.: Cloud condensation nucleation activity of biomass burning aerosol, J. Geophys. Res., 114, https://doi.org/10.1029/2009JD012353, 2009.

Pope, S. B.: Turbulent Flows. Cambridge University Press, 771pp, UK, 2000.

Pósfai, M., Gelencsér, A., Simonics, R., Arató, K., Li, J., Hobbs, P.V., and Buseck, P.R.: Atmospheric tar balls: Particles from biomass and biofuel burning, J. Geophys. Res., 109, https://doi.org/10.1029/2003JD004169, 2004.

Reizer, M., Juda-Rezler, K.: Explaining the high PM_{10} concentrations observed in Polish urban areas, Air Qual. Atmos Health., 9 (5), 517-531, https://doi.org/10.1007/s11869-015-0358-z. 2015.

Rost, J., Holst, T., Sähn, E., Klingner, M., Anke, K., Ahrens, D., and Mayer, H.: Variability of PM10 concentrations dependent on meteorological conditions, Intern. J. Environ. Poll., 36, 3-18, https://doi.org/10.1504/IJEP.2009.021813, 2009.

Sakai, T., Nagai, T., Zaizen, Y., and Mano, Y.: Backscattering linear depolarization ratio measurements of mineral, sea-salt, and ammonium sulfate particles simulated in a laboratory chamber, Appl. Opt., 49, 4441-4449, https://doi.org/10.1364/AO.49.004441, 2010.

Sicard, M., Rocadenbosch, F., Reba, M. N. M., Comerón, A., Tomás, S., García-Vízcaino, D., Batet, O., Barrios, R., Kumar, D., and Baldasano, J. M.: Seasonal variability of aerosol optical properties observed by means of a Raman lidar at an EARLINET site over Northeastern Spain, Atmos. Chem. Phys., 11, 175-190, https://doi.org/10.5194/acp-11-175-2011, 2011.

Sicard, M., Izquierdo, R., Alarcón, M., Belmonte, J., Comerón, A., and Baldasano, J. M.: Near-surface and columnar measurements with a micro pulse lidar of atmospheric pollen in Barcelona, Spain, Atmos. Chem. Phys., 16, 6805-6821, https://doi.org/10.5194/acp-16-6805-2016, 2016.

Siomos, N., Balis, D. S., Poupkou, A., Liora, N., Dimopoulos, S., Melas, D., Giannakaki, E., Filioglou, M., Basart, S., and Chaikovsky, A.: Investigating the quality of modeled aerosol profiles based on combined lidar and sunphotometer data, Atmos. Chem. Phys., 17, 7003-7023, https://doi.org/10.5194/acp-17-7003-2017, 2017.

Siomos, N., Balis, D. S., Voudouri, K. A., Giannakaki, E., Filioglou, M., Amiridis, V., Papayannis, A., and Fragkos, K.: Are EARLINET and AERONET climatologies consistent? The case of Thessaloniki, Greece, Atmos. Chem. Phys., 18, 11885-11903, https://doi.org/10.5194/acp-18-11885-2018, 2018.

Stachlewska, I. S., Costa-Surós, M., and Althausen, D.: Raman lidar water vapour profiling over Warsaw, Poland, Atmos. Res., 194, 258-267, https://doi.org/10.1016/j.atmosres.2017.05.004, 2017a.

Stachlewska, I.S., Zawadzka, O., and Engelmann, R.: Effect of heat wave conditions on aerosol optical properties derived from satellite and ground-based remote sensing over Poland, Remote Sens., 9, 1199, https://doi.org/10.3390/rs9111199, 2017b.

Stachlewska, I. S., Samson, M., Zawadzka, O., Harenda, K. M., Janicka, L., Poczta, P., Szczepanik, D., Heese, B., Wang, D., and Borek, K. Tetoni, E., Proestakis, E., Siomos, N., Nemuc, A., Chojnicki, B.H., Markowicz, K.M., Pietruczuk, A.,

Szkop, A., Althausen, D., Stebel, K., Schuettemeyer, D., and Zehner, C.: Modification of local urban aerosol properties by long-range transport of biomass burning aerosol, Remote Sens., 10, 412, https://doi.org/10.3390/rs10030412, 2018.

Stocker, T., Qin, D., Plattner, G., Tignor, M., Allen, S., Boschung, J., Nauels, A., Xia, Y., Bex, V., and Midgley, P.: IPCC, 2013: Climate Change 2013: The Physical Science Basis. Contribution of Working Group I to the Fifth Assessment Report of the Intergovernmental Panel on Climate Change, Cambridge Univ. Press, Cambridge, UK, and New York, 1535 pp., 2013.

Szczepanik, D. and Markowicz, K.: The relation between columnar and surface aerosol optical properties in a background environment, Atmos. Poll. Res., 9, 246-256, https://doi.org/10.1016/j.apr.2017.10.001, 2018.

Szkop, A. and Pietruczuk, A.: Analysis of aerosol transport over southern Poland in August 2015 based on a synergy of remote sensing and backward trajectory techniques, J. Appl. Remote. Sens., 11, 016039, https://doi.org/10.1117/1.JRS.11.016039, 2017.

Schäfer, K., Emeis, S., Hoffmann, H., and Jahn, C.: Influence of mixing layer height upon air pollution in urban and sub-urban areas, Meteorol. Z., 15 (12), 647-658, https://doi.org/10.1127/0941-2948/2006/0164, 2006.

Sharma, A., Mandal, T., Sharma, S., Shukla, D., and Singh, S.: Relationships of surface ozone with its precursors, particulate matter and meteorology over Delhi, J. Atmos. Chem., 74, 451-474, https://doi.org/10.1007/s10874-016-9351-7, 2017.

Stull, R.B: An introduction to boundary layer meteorology. Springer Science & Business Media: Vol. 13, Dordrecht, 2012.

The EARLINET publishing group 2000-2015.: EARLINET All 2000-2015. World Data Center for Climate (WDCC) at DKRZ. https://doi.org/10.1594/WDCC/EARLINET_All_2000-2015, 2018.

Tian, P., Cao, X., Zhang, L., Sun, N., Sun, L., Logan, T., Shi, J., Wang, Y., Ji, Y., Lin, Y., Huang, Z., Zhou, T., Shi, Y., and Zhang, R.: Aerosol vertical distribution and optical properties over China from long-term satellite and ground-based remote sensing, Atmos. Chem. Phys., 17, 2509-2523, https://doi.org/10.5194/acp-17-2509-2017, 2017.

Trickl, T., Vogelmann, H., Flentje, H., and Ries, L.: Stratospheric ozone in boreal fire plumes – the 2013 smoke season over central Europe, Atmos. Chem. Phys., 15, 9631-9649, https://doi.org/10.5194/acp-15-9631-2015, 2015.

Tang, I. N.: Chemical and size effects of hygroscopic aerosols on light scattering coefficients, J. Geophys. Res., 101, 19245–19250, https://doi.org/10.1029/96JD03003, 1996.

Wałaszek, K., Kryza, M., and Werner, M.: The role of precursor emissions on ground level ozone concentration during summer season in Poland, J. Atmos. Chem., 75, 181-204, https://doi.org/10.1007/s10874-017-9371-y, 2018.

Wandinger, U., Freudenthaler, V., Baars, H., Amodeo, A., Engelmann, R., Mattis, I., Groß, S., Pappalardo, G., Giunta, A., D'Amico, G., Chaikovsky, A., Osipenko, F., Slesar, A., Nicolae, D., Belegante, L., Talianu, C., Serikov, I., Linné, H., Jansen, F., Apituley, A., Wilson, K. M., de Graaf, M., Trickl, T., Giehl, H., Adam, M., Comerón, A., Muñoz-Porcar, C., Rocadenbosch, F., Sicard, M., Tomás, S., Lange, D., Kumar, D., Pujadas, M., Molero, F., Fernández, A. J., Alados-Arboledas, L., Bravo-Aranda, J. A., Navas-Guzmán, F., Guerrero-Rascado, J. L., Granados-Muñoz, M. J., Preißler, J., Wagner, F., Gausa, M., Grigorov, I., Stoyanov, D., Iarlori, M., Rizi, V., Spinelli, N., Boselli, A., Wang, X., Lo Feudo, T., Perrone, M. R., De Tomasi, F., and Burlizzi, P.: EARLINET instrument intercomparison campaigns: overview on strategy

and results, Atmos. Meas. Tech., 9, 1001-1023, https://doi.org/10.5194/amt-9-1001-2016, 2016.

Wang, D., Stachlewska, I. S., Song, X., Heese, B., and A.Nemuc: Variability of boundary layer over an urban continental site based on 10 years of active remote sensing observations in Warsaw, Remote Sens., in review, 2018.

Wang, J. and Christopher, S. A.: Intercomparison between satellite-derived aerosol optical thickness and PM2.5 mass: Implications for air quality studies, Geophys. Res. Lett., 30, 2095, https://doi.org/10.1029/2003GL018174, 2003.

Xie, C., Nishizawa, T., Sugimoto, N., Matsui, I., and Wang, Z.: Characteristics of aerosol optical properties in pollution and Asian dust episodes over Beijing, China, Appl. Opt., 47, 4945-4951, https://doi.org/10.1364/AO.47.004945, 2008.

Zawadzka, O., Markowicz, K., Pietruczuk, A., Zielinski, T., and Jaroslawski, J.: Impact of urban pollution emitted in Warsaw on aerosol properties. Atmos. Environ., 69, 15-28, https://doi.org/10.1016/j.atmosenv.2012.11.065, 2013.

Zhang, H., Wang, Y., Hu, J., Ying, Q., and Hu, X.-M.: Relationships between meteorological parameters and criteria air pollutants in three megacities in China. Environ. Res., 140, 242-254, https://doi.org/10.1016/j.envres.2015.04.004, 2015.

Zang, Z. L., Wang, W. Q., You, W., Li, Y., Ye, F., and Wang, C. M.: Estimating ground-level PM2.5 concentrations in Beijing, China using aerosol optical depth and parameters of the temperature inversion layer, Sci. Total Environ., 575, 1219–1227, https://doi.org/10.1016/j.scitotenv.2016.09.186, 2017.

Zheng, S., Pozzer, A., Cao, C. X., and Lelieveld, J.: Long-term (2001–2012) concentrations of fine particulate matter ($PM_{2.5}$) and the impact on human health in Beijing, China, Atmos. Chem. Phys., 15, 5715-5725, https://doi.org/10.5194/acp-15-5715-2015, 2015.

TABLES

Table 1 Literature revive based values of lidar-derived particle optical properties used for the interpretation of the aerosol measured over the RS-Lab in Warsaw. The listed properties are assigned to each aerosol layer based on manual approach in combination with case-to-case air-mass transport analyses.

	LR [sr]		δ [%]		ÅE	RH	Air-mass transport *	No. of cases (in ABL) [%]
	355	532	355	532	(355/532)	[%]		
Anthropogenic pollution	50-65	33-72	3-6	3-11	0.7-1.8	50-90	Local (Warsaw) Advective (Western Europe)	151 (61%)
Biomass burning	50-95	60-90	2-6	4-12	0.8-2.0	60-80	Advective (Eastern Europe, North America)	34 (14%)
Pollen	50-75	46-69	5-17	6-20	---	< 50	Local	16 (7%)
Arctic marine	16-30	18-26	1-7	1-11	-0.6-0.7	---	Arctic, subarctic	14 (5%)
Dust	50-70	45-65	24-29	25-43	0.1-1.5	20-40	Advective (Africa)	0
Undefined Mixtures								31 (13%)

* Calculations up to 10 days backward-trajectories for aerosol layers in free troposphere and in boundary layer, assessment of possible source of aerosols, interpreting it against satellite data and model outputs (eg: MODIS, MSG, CALIPSO, NAAPS).

Table 2. Mean values of the aerosol optical properties with standard deviations derived within aerosol boundary layer (ABL) from PollyXT lidar at the EARLINET site in Warsaw for measurements at 355 and 532 nm conducted in period of July-September of 2013, 2015, and 2016. Symbols denote: particle extinction coefficient (α), particle backscatter coefficient (β), aerosol optical depth (AOD), lidar ratio (LR), particle linear depolarization ratio (δ), Ångstrom exponent (ÅE) and aerosol boundary layer height (ABLH). Mean values are obtained for different time of day with respect to the boundary layer type.

	λ (nm)	α_{ABL} (Mm^{-1})	β_{ABL} ($Mm^{-1}sr^{-1}$)	AOD_{ABL}	LR_{ABL} (sr)	δ_{ABL}	$ÅE_{ABL}$	ABLH (km)
Entire time (ET)								
WML, RL, MTL (246 cases)	355	142 ±68	3.1±1.2	0.20±0.10	48±17	0.02±0.01	1.54±0.37	1.33±0.36
	532	83 ±43	2.2±0.7	0.11±0.06	41±15	0.05±0.01		
Nocturnal time (NT) [21:00-2:00 UTC]								
NL (113 cases)	355	129±56	3.0±1.1	0.11±0.04	44±12	0.02±0.01	1.58±0.36	0.76±0.12
	532	69±39	1.9±0.7	0.07±0.02	38±12	0.05±0.01		
RL (105 cases)	355	137±53	3.1±1.0	0.18±0.08	47±15	0.02±0.01	1.61±0.38	1.34±0.17
	532	75±37	2.3±1.0	0.11±0.05	40±13	0.04±0.01		
Transition time (TT) during Sunrise [3:00-8:00 UTC] & Sunset [16:00-20:00 UTC]								
MTL (37 cases)	355	128±54	3.8±1.1	0.11±0.03	37±14	0.02±0.01	1.53±0.30	0.70±0.10
	532	73±35	2.3±0.6	0.06±0.02	32±13	0.04±0.01		
WML (63 cases)	355	163 ±63	2.8±1.1	0.24±0.01	55 ±18	0.02±0.01	1.37±0.34	1.60±0.38
	532	96 ±49	1.9±0.8	0.14±0.05	49±16	0.05±0.02		

Table 3. Mean daytime (3:00-19:00 UTC) aerosol optical depth (AOD) and Ångstrom exponent (ÅE) with standard deviations derived within boundary layer at 355 and 532 nm from PollyXT lidar at the EARLINET site in Warsaw and in atmospheric column measured by MFR-7 shadowband radiometer (415 and 500 nm) at the PolandAOD-NET site in Warsaw. For reference the mean values derived from Level 2.0 CE318 CIMEL (380 and 500 nm) at the AERONET site in Belsk are given. The AOD$_{CL}$ of CE318 and MFR-7 were scaled to the lidar wavelength (respectively 355 and 532 nm) using Ångstrom law. The mean values were obtained for July-September of 2013, 2015, 2016 when instruments operated simultaneously (41 cases). In brackets, the mean values derived for cases with no aerosol in the free-troposphere (10 cases), as given in EARLINET/ACTRIS Data Base.

	AOD	AOD	ÅE(355/532)	ÅE(380/500)	ÅE(415/500)
AERONET Belsk (columnar) reference site		**C318 photometer**			
All cases	**355 nm**	**532nm**			
(no FT aerosol)	0.41±0.17	0.23±0.09	1.49±0.23		
	(*0.31±0.14*)	(*0.19±0.08)*	(*1.58±0.12*)		
	380 nm	**500nm**			
	0.36±0.16	0.24±0.12		1.51±0.23	
	(0.29±*0.11*)	(0.20±*0.07*)		(*1.59±0.10*)	
PolandAOD Warsaw (columnar)		**MFR-7 shadowband radiometer**			
All cases	**355 nm**	**532 nm**			
(no FT aerosol)	0.45±0.17	0.25±0.11	1.56±0.21		
	(*0.29±0.09*)	(*0.15±0.05*)	(*1.60±0.15*)		
	415 nm	**500 nm**			
	0.36±0.15	0.27±0.12			1.50±0.31
	(0.25±*0.07*)	(0.17±*0.05*)			(*1.62±0.33*)
EARLINET Warsaw (within aerosol boundary)		**PollyXT-UW Raman lidar**			
All cases	**355nm**	**532nm**			
(no FT aerosol)	0.20±0.06	0.13±0.03	1.53±0.23		
	(*0.19±0.07*)	(*0.12±0.04*)	(*1.59±0.16*)		

FIGURES

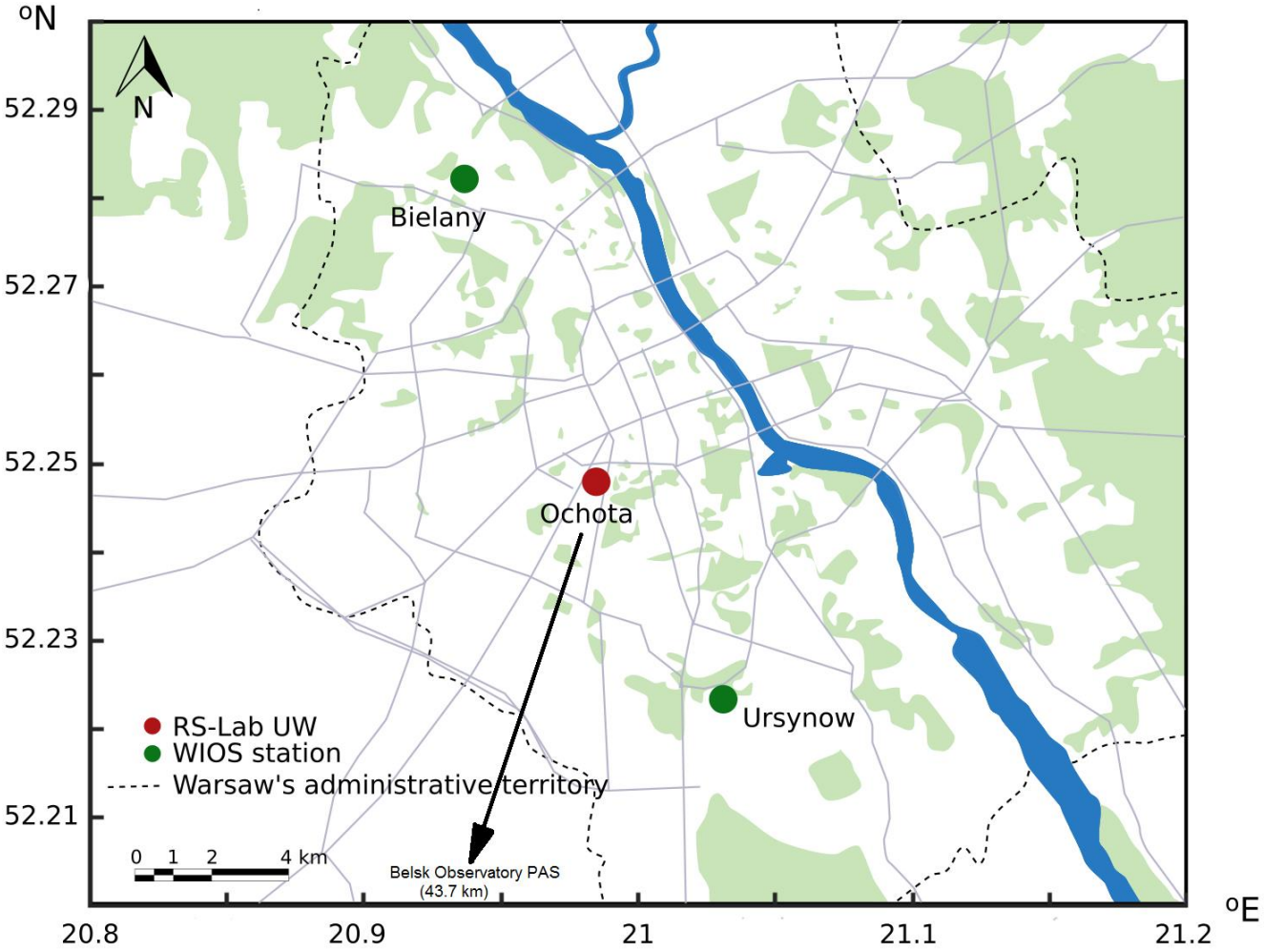

Figure 1. The location of the Remote Sensing Laboratory at UW Ochota Campus in Warsaw, the WIOS monitoring station in Ursynow and Bielany, and the IGF-PAN Observatory in Belsk.

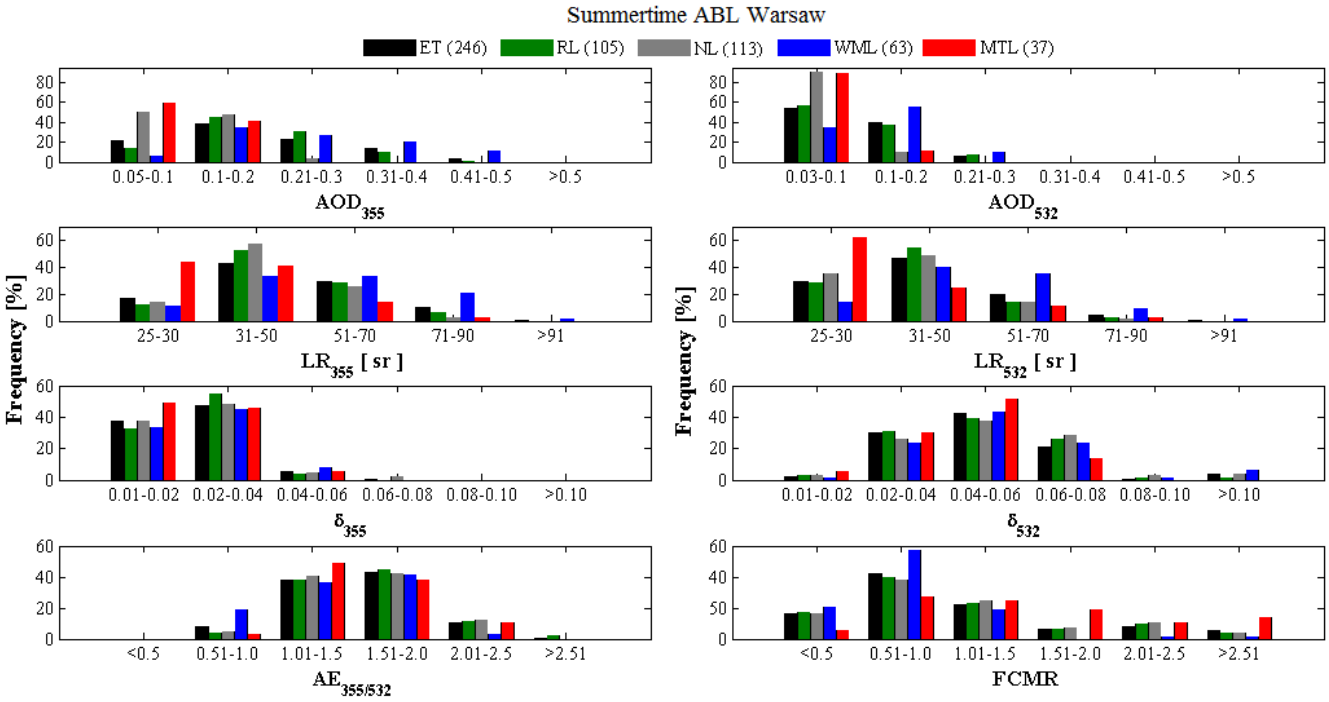

Figure 2. Frequency distribution of aerosol optical depth (AOD), lidar ratio (LR), particle linear depolarization ratio (δ) and Ångstrom exponent (ÅE) at 355 and 532 nm, derived within aerosol boundary layer at the EARLINET lidar site in Warsaw for period of July-September 2013, 2015, 2016 with corresponding fine to coarse mass ratio (FCMR) derived from surface particulate matter with an aerodynamic diameter below 10µm (PM_{10}) and below 2.5µm ($PM_{2.5}$) measurements at the WIOS site in Warsaw-Ursynow. The period of measurement is divided to the entire time (ET; 24 h), the nocturnal time (NT; 22:00-2:00 UTC, including the residual boundary layer RL and nocturnal boundary layer NL) and the transition time (TT; after sunrise at 03:00-8:00 for morning transition layer MTL and before sunset at 16:00-20:00 UTC for well-mixed boundary layer WML).

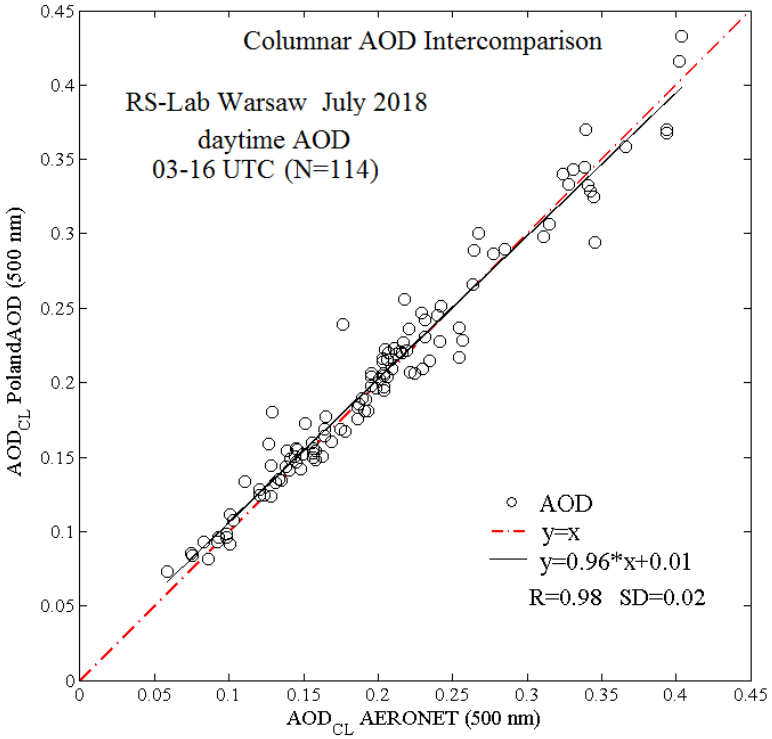

Figure 3. Intercomparison of hourly averaged clear-sky daytime aerosol optical depth measured within the atmospheric column(AOD_{CL}) with CE318 at the AERONET site (Level 2.0 data) and the MFR-7 shadowband radiometer at the PolandAOD-NET site (Level 1.5 data) show high agreement for a month of collocated measurements at the RS-Lab in Warsaw.

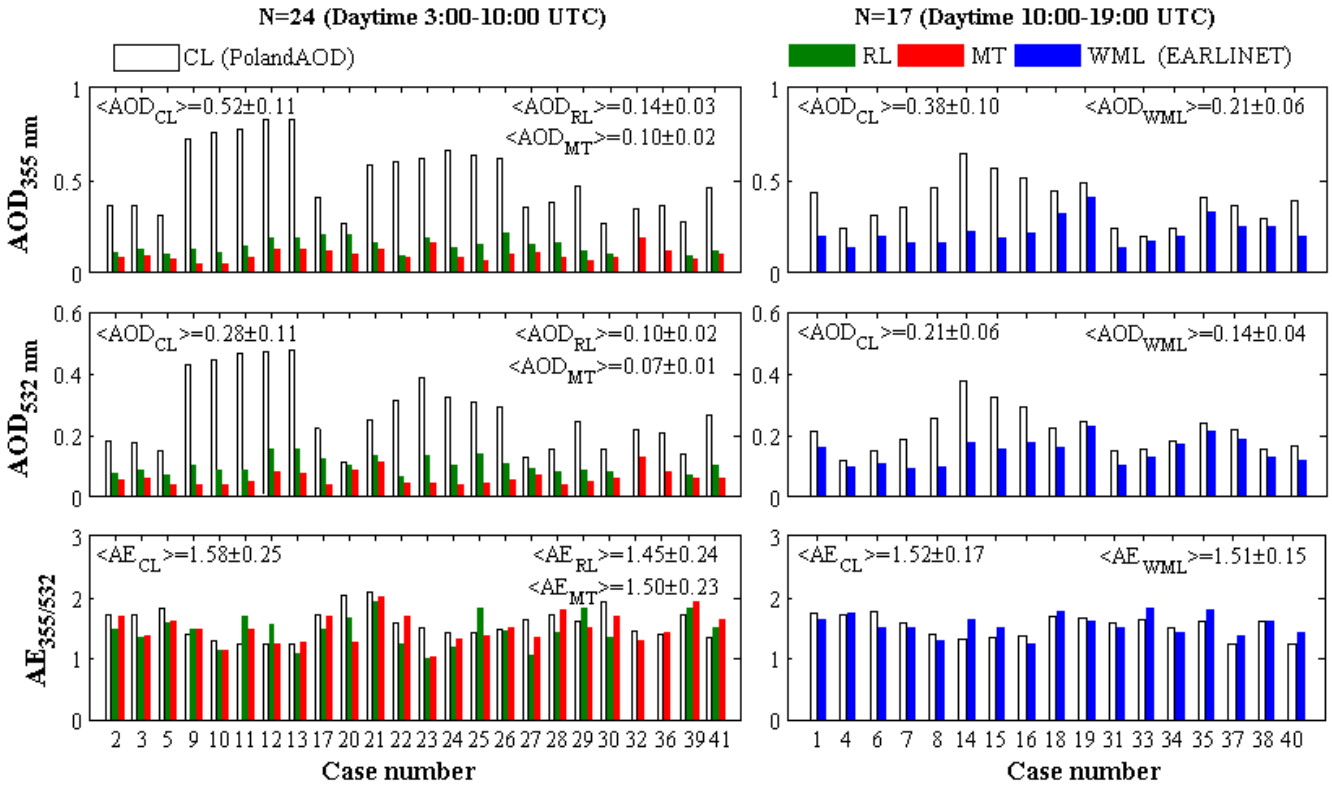

Figure 4. Hourly averages of aerosol optical depth (AOD) and Ångstrom exponent (ÅE) derived within boundary layer at 355 and 532 nm from PollyXT lidar at the EARLINET site in Warsaw and corresponding MFR-7 shadowband radiometer at the PolandAOD-NET site in Warsaw for July-September 2013, 2015, 2016 (leap year). AOD_{CL} of MFR-7 measurements at 415 and 500 nm were scaled to 355 and 532 nm using Ångstrom law.

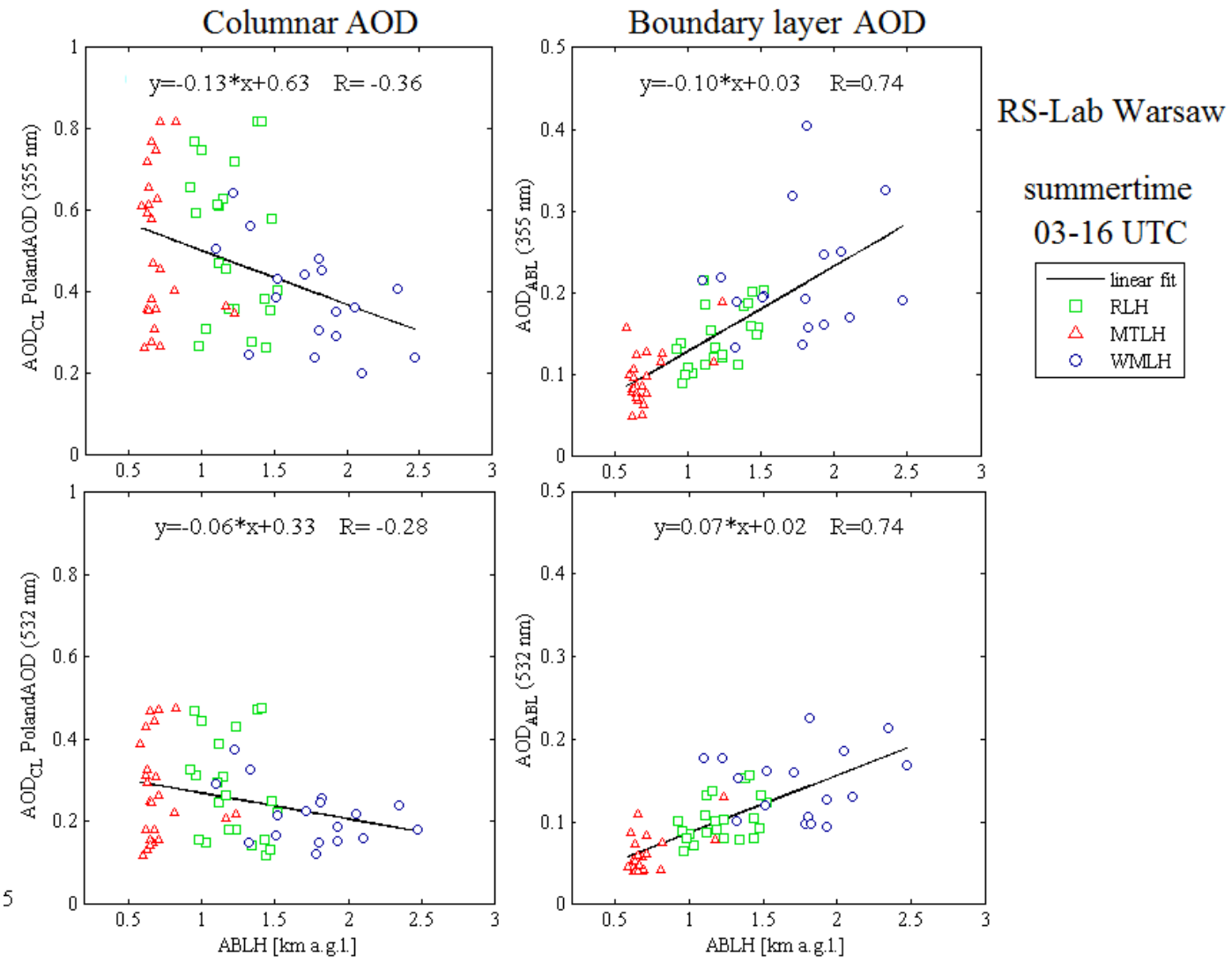

Figure 5. Opposite relation of the MFR-7 columnar AOD versus boundary layer AOD derived at 355 and 532 nm from PollyXT lidar at the EARLINET site in Warsaw (right), against the lidar derived aerosol boundary layer height (ABLH) in Warsaw for summertime period of July-September of 2013, 2015, 2016. Note that AOD_{CL} of MFR-7 was scaled using the law from 415 and 500 nm to match lidar's 355 and 532 nm, respectively.

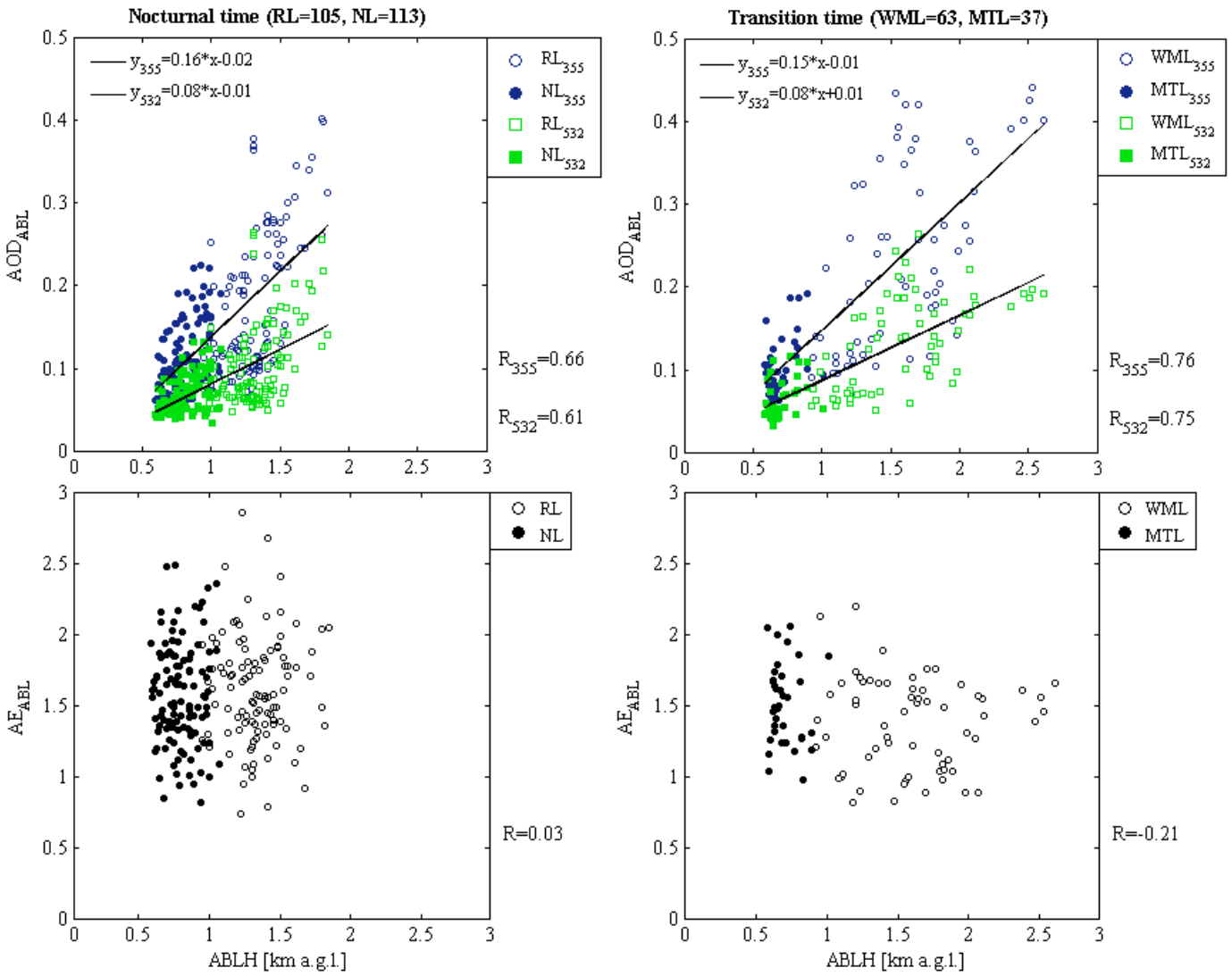

Figure 6. Comparison of hourly averaged aerosol optical depth (AOD) and Ångstrom exponent (ÅE) derived within boundary layer at 355 and 532 nm against aerosol boundary layer height (ABLH) derived from PollyXT lidar at the EARLINET site in Warsaw in period of July-September of 2013, 2015, 2016. Linear fit to data points is shown for correlation coefficients R > 0.6.

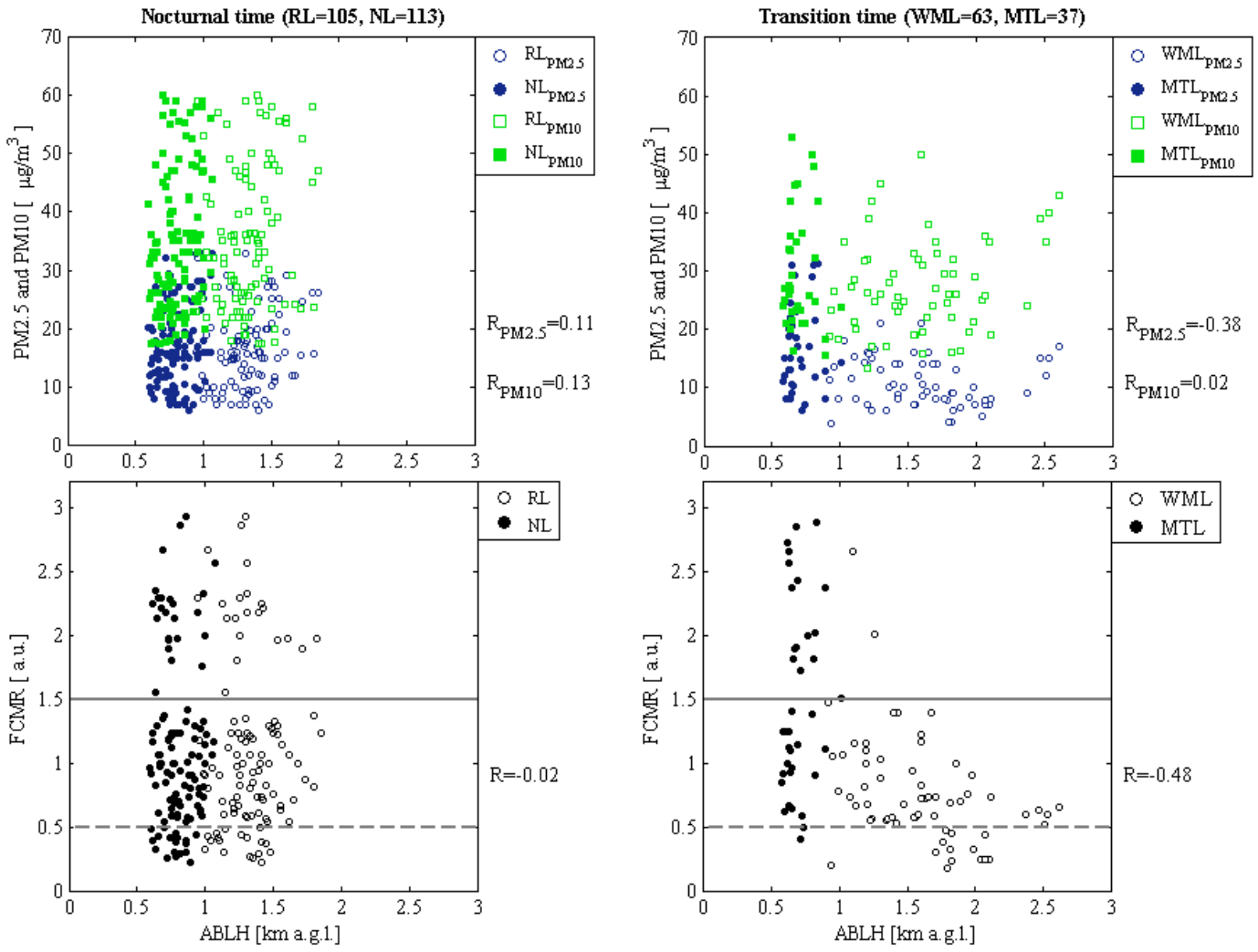

Figure 7. Comparison of hourly averages of surface fine to coarse mass ratio (FCMR), and particulate matter ($PM_{2.5}$ and PM_{10}) measured at the WIOS site in Warsaw-Ursynow with aerosol boundary layer height (ABLH) derived from PollyXT lidar at the EARLINET site in Warsaw in period of July-September of 2013, 2015, 2016. Thresholds of FCMR are marked as horizontal lines.

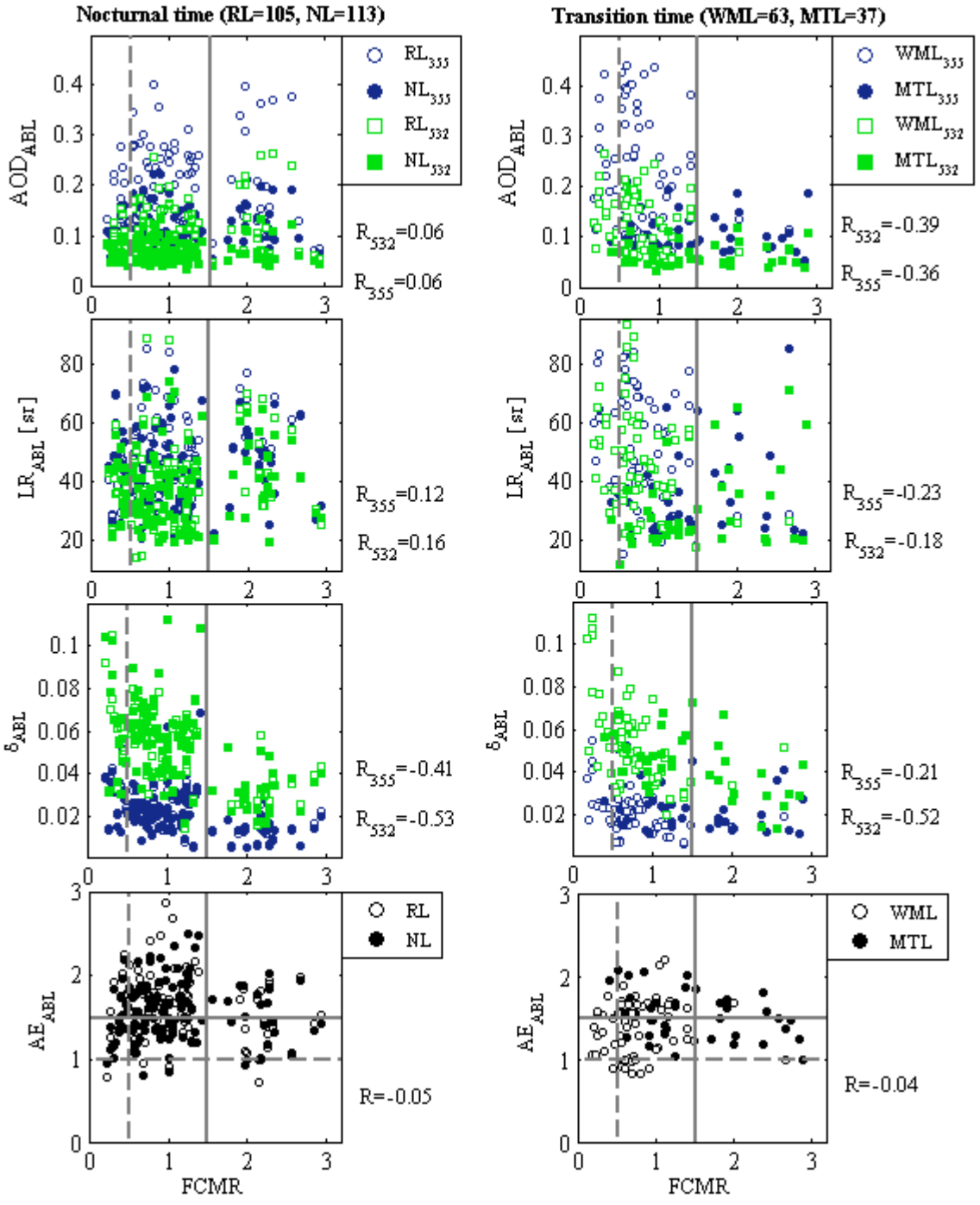

Figure 8. Comparison of hourly averaged aerosol optical depth (AOD), lidar ratio (LR), particle linear depolarization ratio (δ) and Ångstrom exponent (ÅE) derived within boundary layer at 355 and 532 nm of PollyXT lidar at the EARLINET site in Warsaw for July-September of 2013, 2015, 2016 with hourly averages of surface fine to coarse mass ratio (FCMR) derived from particulate matter ($PM_{2.5}$

and PM_{10}) measured at the WIOS site in Warsaw-Ursynow. Thresholds of ÅE and FCMR are marked as horizontal and vertical lines, respectively.

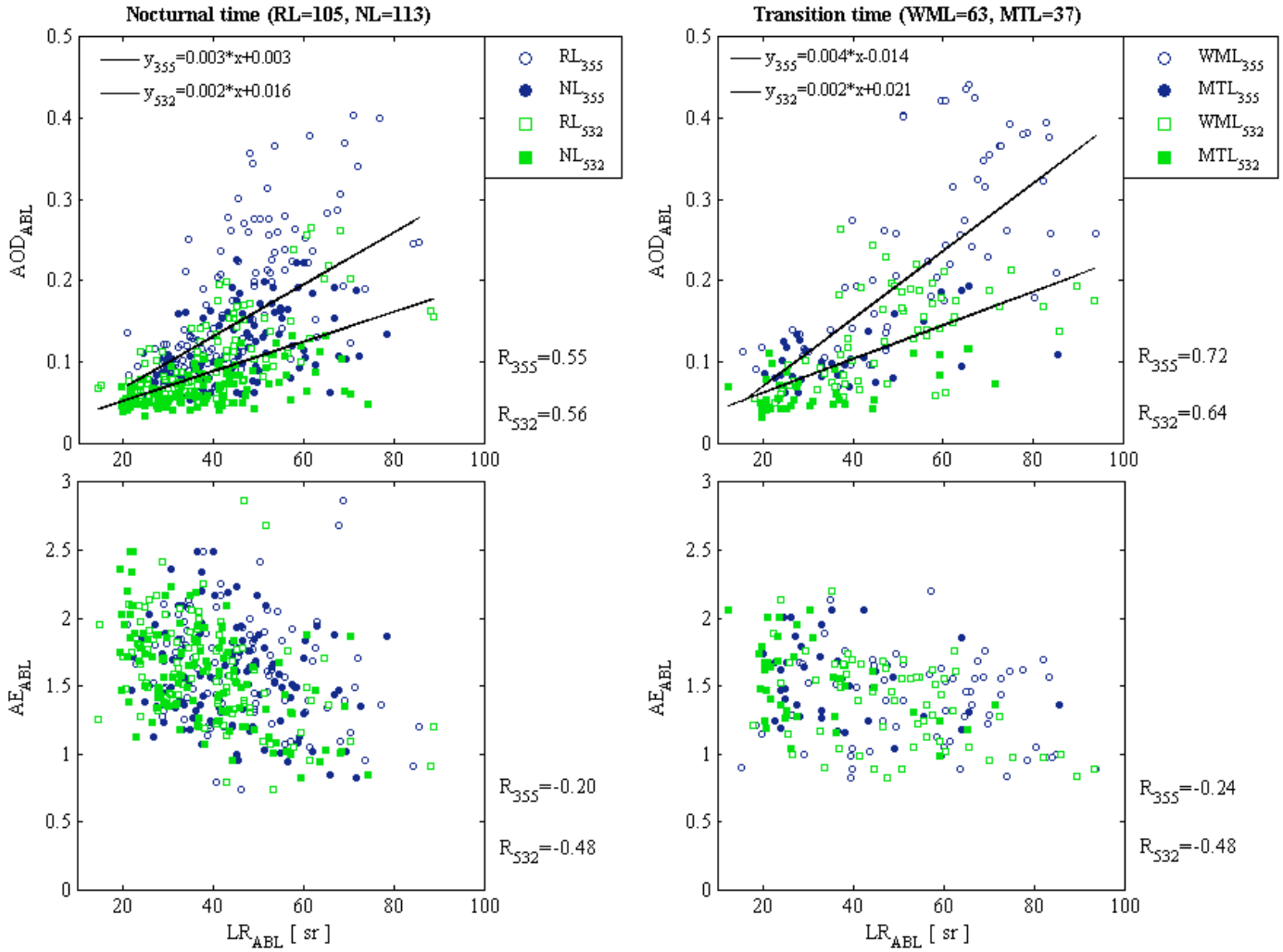

Figure 9. Comparison of hourly averaged aerosol optical depth (AOD), Ångstrom exponent (ÅE), and lidar ratio (LR) derived within boundary layer at 355 and 532 nm from PollyXT lidar at the EARLINET site in Warsaw in period of July-September of 2013, 2015, 2016. Lack of any correlation between linear particle depolarization ratio (δ) and lidar ratio (LR) is not shown for brevity. Linear fit to data points is shown for correlation coefficients R > 0.6.

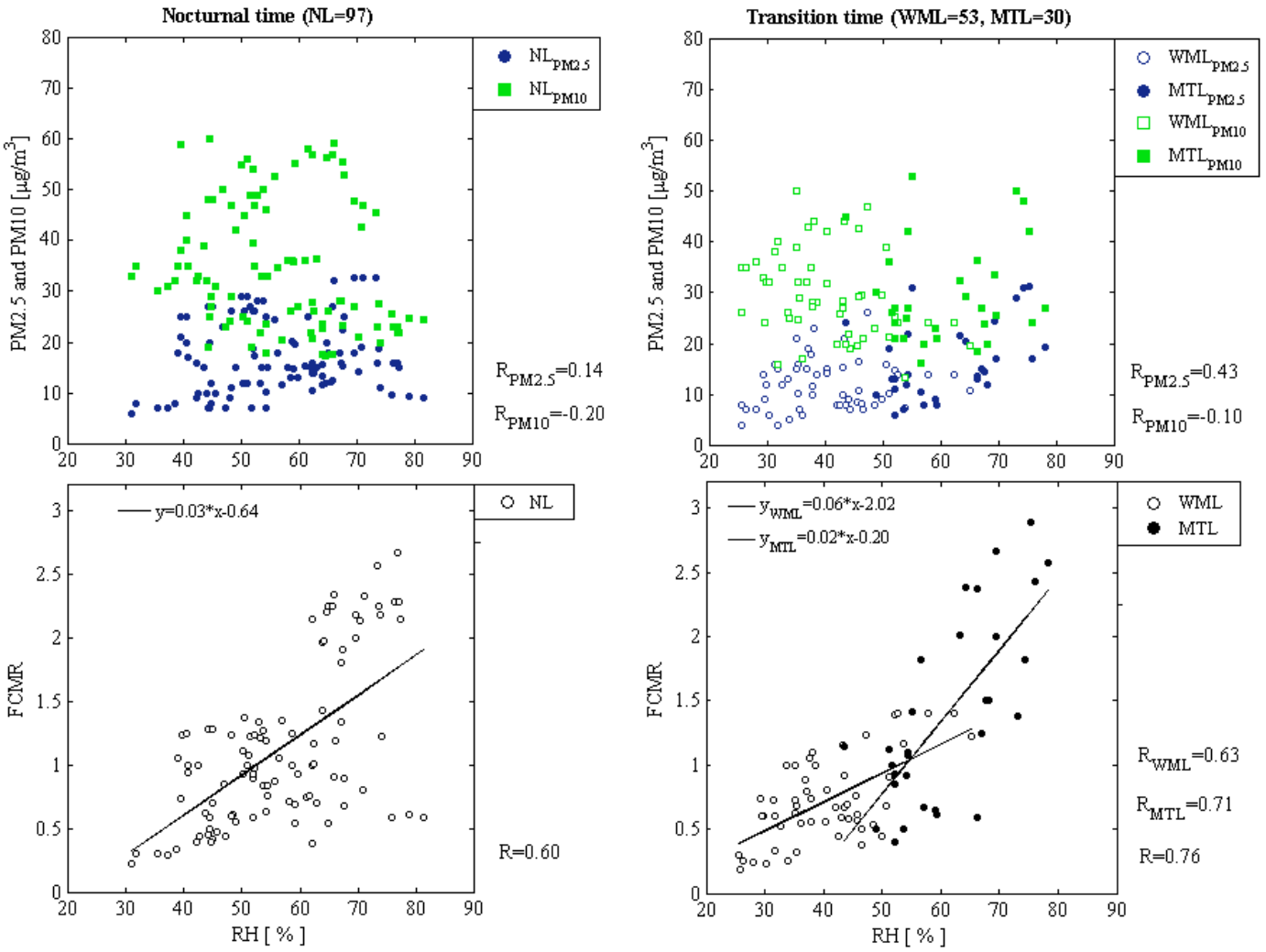

Figure 10. Comparison of the hourly averaged near-surface relative humidity (RH) measured by the weather transmitter WXT510 (Vaisala) in Warsaw in period of July-September of 2013, 2015, 2016 with the hourly averages of surface particulate matter $PM_{2.5}$ and PM_{10} measured at the WIOS site in Warsaw-Ursynow. Linear fit to data points is shown for correlation coefficients R > 0.6.

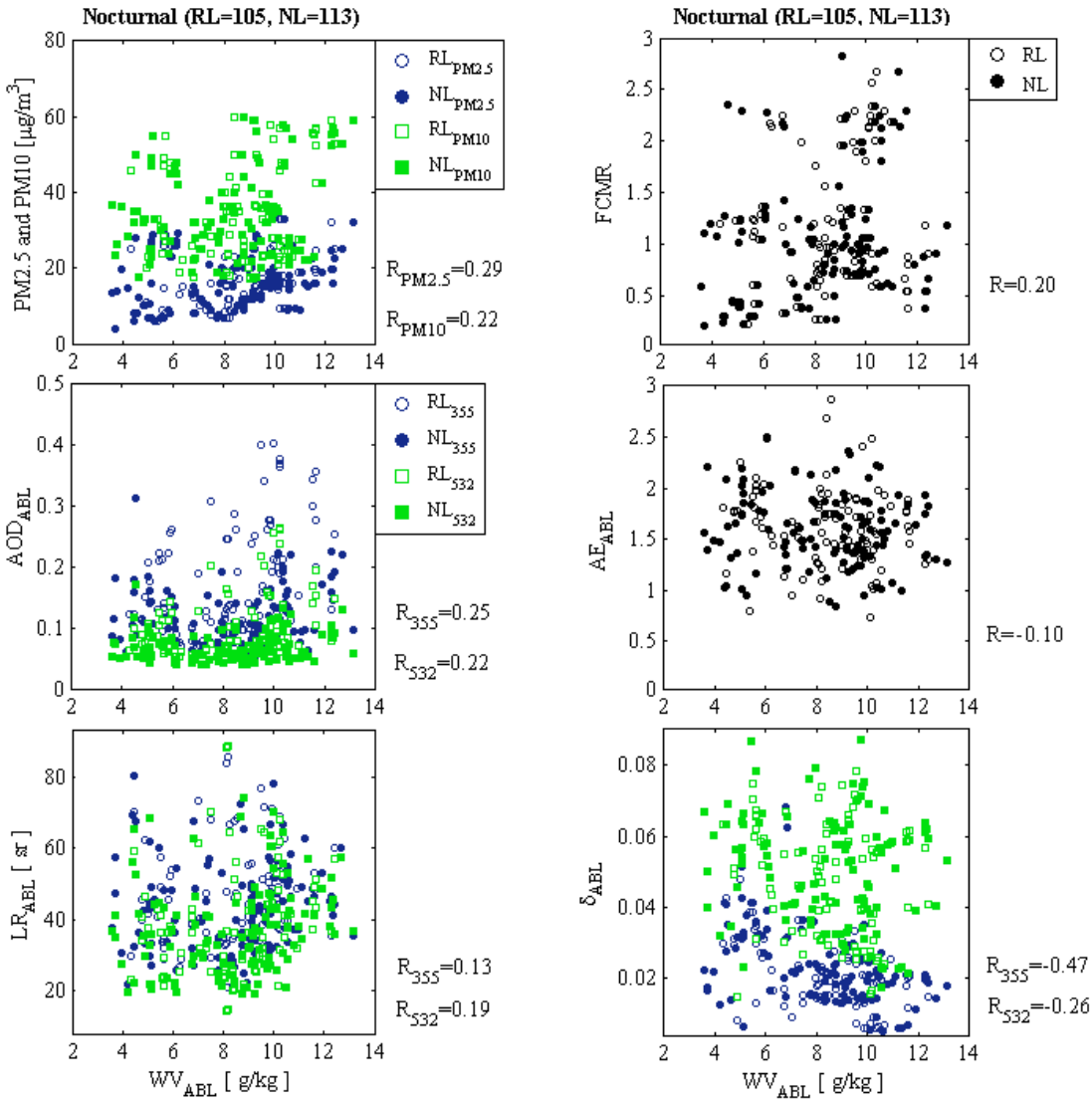

Figure 11. Comparison of Raman lidar derived nighttime hourly water vapour mixing ratio (WV), aerosol optical depth (AOD), lidar ratio (LR), Ångstrom exponent (ÅE) and particle linear depolarization ratio (δ) derived within aerosol boundary layer at the EARLINET site in Warsaw and with the hourly averages of surface particulate matter $PM_{2.5}$ and PM_{10} and fine to coarse mass ratio (FCMR) measured at the WIOS site in Warsaw-Ursynow during period of July-September of 2013, 2015, 2016. NOTE: lidar water vapour available only at nighttime.

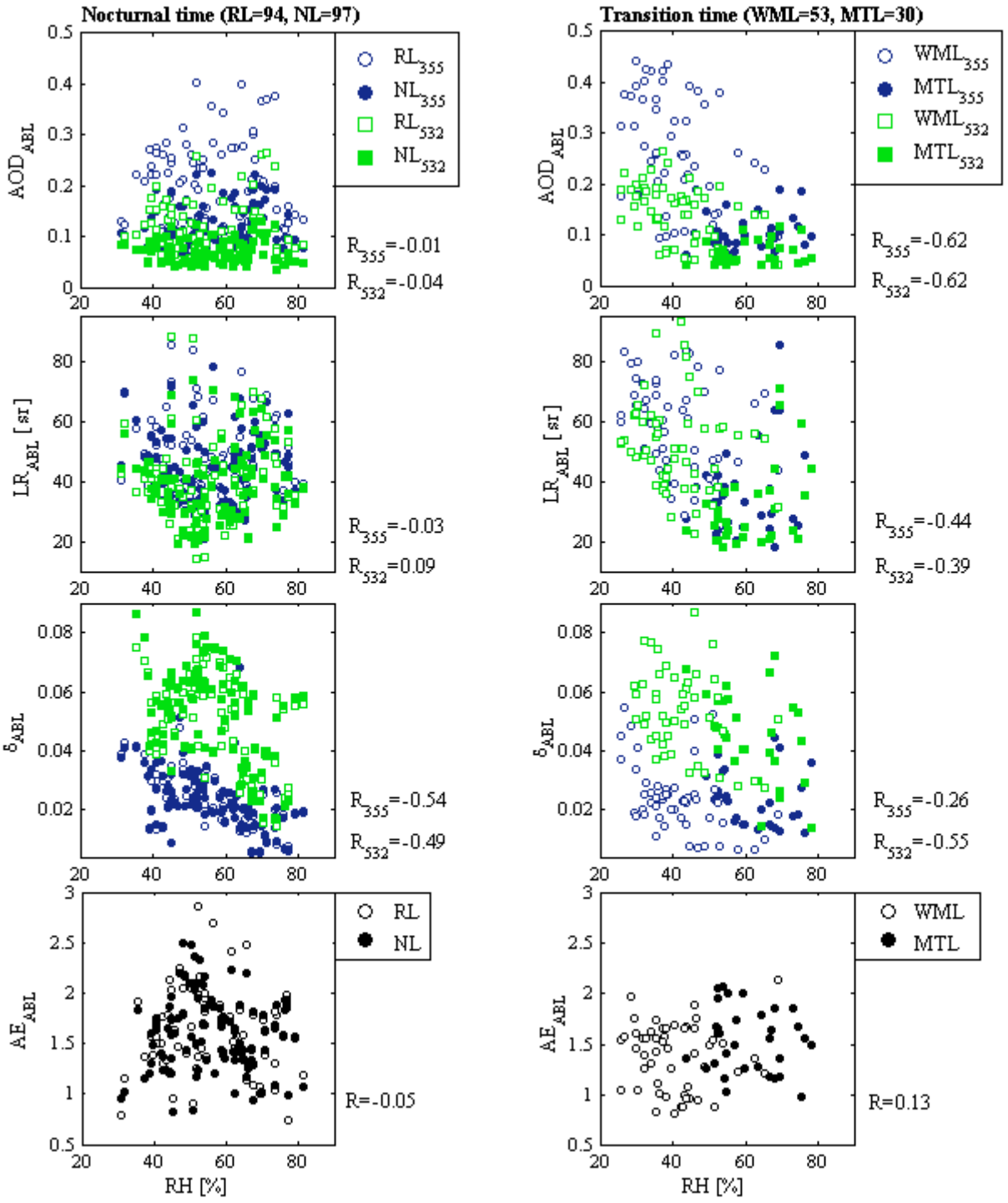

Figure 12. Comparison of hourly averaged near-surface relative humidity (RH) measured by the weather transmitter WXT510 (Vaisala) with wavelength dependent aerosol optical depth (AOD), lidar ratio (LR), particle linear depolarization ratio (δ) and

Ångstrom exponent (ÅE) as derived within boundary layer at 355 and 532 nm from PollyXT lidar at the EARLINET site in Warsaw in period of July-September of 2013, 2015, 2016.